UNLV Theses, Dissertations, Professional Papers, and Capstones

May 2016

The Hopf Fibration and Encoding Torus Knots in Light Fields

John Vincent Waite

University of Nevada, Las Vegas, jvw831@gmail.com

THE HOPF FIBRATION AND ENCODING TORUS KNOTS IN LIGHT FIELDS

By

John Waite

Bachelor of Science - Mathematics
University of Maryland, College Park
2010

A thesis submitted in partial fulfillment
of the requirements for the

Master of Science - Physics

Department of Physics and Astronomy
College of Sciences
The Graduate College

University of Nevada, Las Vegas
May 2016

UNLV | GRADUATE COLLEGE

Thesis Approval

The Graduate College
The University of Nevada, Las Vegas

April 8, 2016

This thesis prepared by

John Waite

entitled

The Hopf Fibration and Encoding Torus Knots in Light Fields

is approved in partial fulfillment of the requirements for the degree of

Master of Science – Physics
Department of Physics and Astronomy

Bernard Zygelman, Ph.D.
Examination Committee Chair

Michael Pravica, Ph.D.
Examination Committee Member

Stephen Lepp, Ph.D.
Examination Committee Member

Dieudonne D. Phanord, Ph.D.
Graduate College Faculty Representative

Kathryn Hausbeck Korgan, Ph.D.
Graduate College Interim Dean

Abstract

The first sections of this thesis explore a construction of electromagnetic fields first proposed by Bateman [2] and recently rediscovered [8] and expanded upon. With this powerful and elegant tool, I show that it is possible to construct families of EM fields that have a common topological structure that is preserved throughout time. This topological structure, known as the Hopf fibration, has been found to manifest itself in many areas of physics. Due to its utility, I have made a detailed study of it. The final section of this thesis develops an algorithm to parameterize a closed, bounded, and oriented surface that has as its boundary a torus knot. These types of surfaces, known as Seifert surfaces [17], contain information about the energy structure of the EM fields developed in the earlier sections of this thesis and may also lead to detection protocols for such fields. Because these surfaces are closed, bounded and oriented then Stokes' theorem should be valid. A verification of this proposition is included.

Acknowledgements

I would like to thank my advisor, Dr. Bernard Zygelman, for the guidance and direction he provided me throughout the entire process of producing this thesis, and also for supplying me with the ideas in the first place.

I would also like to acknowledge the other members of my committee, Drs. Lepp, Pravica, and Phanord, for their patience with me during the weeks leading to my defense.

Finally, I would like to thank my wife, Kelly, for the sacrifices she was required to make in my behalf for the past two years.

Dedication

This thesis is dedicated to my dear wife Kelly. Without your support this project would never have started in the first place.

Table of Contents

List of Figures

1 Introduction

The study of knots has a rich history, dating back to the 1860's when Lord Kelvin proposed his vortex atom hypothesis [18]. Although this hypothesis was eventually abandoned with the discovery of the atom about a decade later, the rigorous study of knots in a mathematical framework was well underway. Until recently, the study of knots was confined almost exclusively to the realm of pure mathematics. Knots, and their intrinsic topological properties, have again entered the domain of mainstream theoretical physics.

The remarkable aspect of the solutions of Maxwell's equations we will investigate are their stablity in time, and that they possess a topological invariant, in that the electric and magnetic field lines are linked for all time, and the Poynting field line structure is unchanged in time. This topological structure could be exploited in many applications. The study of topological invariants has recently gained ground in many branches of physics research. Notably, the advances made in the field of quantum computation and information have yielded promising results that utilize the topological nature of light and matter [4,10]. While much of this research is still confined to the realm of theoretical physics, it will not be long before these phenomenon may be realized in the laboratory. This recent activity has resulted in a large increase in the funding available for continued research and development.

The solutions studied in this paper are confined to the realm of electromagnetic radiation, but it would not be prudent to limit the study of such solutions to light. There is no reason to assume that these types of solutions could not be applied to matter as well. The reason that such topological invariants are important to such branches of study such as quantum information lies in the stability and robustness of that topology. These types of invariants are nearly immune to noise and perturbations, making them ideal candidates for information storage and use as qubits, as they are essentially deaf to sources of decoherence.

In Chapter 2, I will present the construction proposed by Bateman [2]. Chapter 3 will verify the validity of this construction on a familiar solution to Maxwell's equations in free space. Chapters 4 and 5 provide some background on tori and a presentation of the structure

referred to as the Hopf fibration. Chapter 6 will examine the solutions proposed by Kedia et al. [8]. Finally, Chapter 7 will present an algorithm to parameterize Seifert surfaces and verify Stokes' theorem on one such surface.

2 Bateman's Construction

2.1 Motivation

The usual solutions to Maxwell's equations we encounter are plane waves. These solutions, while important and useful, are only a small subset of the total solutions that are allowed. Finding and developing solutions to the wave equation has been a part of physics education and continuing research for the past 150 years. The reason for this restricted subset of solutions arises from the methods used to solve the resulting wave equation. It is typical to use the method of separation of variables to find solutions. However, there is no fundamental reason for all solutions to be separable. With the advances made in technology, specifically in computation, we have been able to shed light on and further our understanding of these non-separable solutions. One of the basic principles that makes this field a nearly inexhaustible one is the fact that the superposition of solutions is also a solution. This principle of superposition, and accounting for various boundary conditions, is vital when we attempt to create new solutions from old ones.

The following derivation explores another method to solving the wave equation.

2.2 Derivation

The method outlined in the thesis uses the construction of an electromagnetic field proposed by Bateman [2] as early as 1915. This construction goes as follows. We begin with Maxwell's equations in free space. These equations are familiar

$$\nabla \times \mathbf{B} = \frac{\partial \mathbf{E}}{\partial t} = \partial_t \mathbf{E} \qquad \text{and} \qquad \nabla \times \mathbf{E} = -\frac{\partial \mathbf{B}}{\partial t} = -\partial_t \mathbf{B} \tag{1}$$

along with the sourceless conditions

$$\nabla \cdot \mathbf{B} = 0 \qquad \text{and} \qquad \nabla \cdot \mathbf{E} = 0 \tag{2}$$

3

Here, we have adopted units such that $c = 1$. At this point, we construct a new field represented by $\mathbf{F}$ and defined as

$$\mathbf{F} \equiv \mathbf{E} + \imath \mathbf{B} \tag{3}$$

where $\imath = \sqrt{-1}$ is the usual complex number, and the fields represented by $\mathbf{E}$ and $\mathbf{B}$ are, themselves, solutions to Maxwell's equations. This vector is the Riemann-Silberstein vector [8] and is also referred to as the electromagnetic field, and Maxwell's equations can be written as

$$\nabla \times \mathbf{F} = \nabla \times \mathbf{E} + \imath \left(\nabla \times \mathbf{B} \right) = -\partial_t \mathbf{B} + \imath \partial_t \mathbf{E} = \imath \partial_t \left(\mathbf{E} + \imath \mathbf{B} \right) = \imath \partial_t \mathbf{F}$$

and

$$\nabla \cdot \mathbf{F} = \nabla \cdot \mathbf{E} + \imath (\nabla \cdot \mathbf{B}) = 0 + \imath \cdot 0 = 0$$

So, now we have that Maxwell's equations can be written in terms of this new vector $\mathbf{F}$ as follows

$$\nabla \times \mathbf{F} = \imath \partial_t \mathbf{F} \qquad \text{and} \qquad \nabla \cdot \mathbf{F} = 0 \tag{4}$$

The next step in the construction is to find two complex scalar functions $\alpha(x, y, z, t)$ and $\beta(x, y, z, t)$ such that

$$\nabla \alpha \times \nabla \beta = \imath \left(\partial_t \alpha \, \nabla \beta - \partial_t \beta \, \nabla \alpha \right) \tag{5}$$

This condition is equivalent to the following conditions

$$(\partial_x \alpha)^2 + (\partial_y \alpha)^2 + (\partial_z \alpha)^2 - (\partial_t \alpha)^2 = (\nabla \alpha)^2 - (\partial_t \alpha)^2 = 0$$

$$(\partial_x \beta)^2 + (\partial_y \beta)^2 + (\partial_z \beta)^2 - (\partial_t \beta)^2 = (\nabla \beta)^2 - (\partial_t \beta)^2 = 0 \tag{6}$$

$$\partial_x \alpha \partial_x \beta + \partial_y \alpha \partial_y \beta + \partial_z \alpha \partial_z \beta - \partial_t \alpha \partial_t \beta = \nabla \alpha \cdot \nabla \beta - \partial_t \alpha \, \partial_t \beta = 0$$

To see how these conditions are equivalent, we consider the x-component of $\nabla \alpha \times \nabla \beta$ as

4

follows

$$(\nabla\alpha \times \nabla\beta)_x = \partial_y\alpha\,\partial_z\beta - \partial_y\beta\,\partial_z\alpha = \frac{\partial(\alpha,\beta)}{\partial(y,z)}$$

Now, if we square this term we get that

$$(\partial_y\alpha\,\partial_z\beta - \partial_y\beta\,\partial_z\alpha)^2 = \partial_y\alpha^2\partial_z\beta^2 + \partial_y\beta^2\partial_z\alpha^2 - 2\partial_y\alpha\partial_y\beta\partial_z\alpha\partial_z\beta$$

$$= \left(\partial_y\alpha^2 + \partial_z\alpha^2\right)\left(\partial_y\beta^2 + \partial_z\beta^2\right)$$

$$- \partial_y\alpha^2\partial_y\beta^2 - \partial_y\beta^2\partial_z\alpha^2 - 2\partial_y\alpha\partial_z\alpha\partial_y\beta\partial_z\beta$$

$$= \left(\partial_y\alpha^2 + \partial_z\alpha^2\right)\left(\partial_y\beta^2 + \partial_z\beta^2\right) - (\partial_y\alpha\partial_y\beta + \partial_z\alpha\partial_z\beta)^2$$

and using (6) we get that

$$= \left(\partial_t\alpha^2 - \partial_x\alpha^2\right)\left(\partial_t\beta^2 - \partial_x\beta^2\right) - (\partial_t\alpha\partial_t\beta - \partial_x\alpha\partial_x\beta)^2$$

expanding these expressions we get

$$= \cancel{\partial_t\alpha^2\partial_t\beta^2} - \partial_t\alpha^2\partial_x\beta^2 - \partial_t\beta^2\partial_x\alpha^2 + \cancel{\partial_x\alpha^2\partial_x\beta^2}$$

$$- \cancel{\partial_t\alpha^2\partial_t\beta^2} - \cancel{\partial_x\alpha^2\partial_x\beta^2} + 2\partial_t\alpha\partial_t\beta\partial_x\alpha\partial_x\beta$$

$$= -\left(\partial_t\alpha^2\partial_x\beta^2 + \partial_t\beta^2\partial_x\alpha^2 - 2\partial_t\alpha\partial_t\beta\partial_x\alpha\partial_x\beta\right)$$

$$= -\left(\partial_t\alpha\partial_x\beta - \partial_t\beta\partial_x\alpha\right)^2$$

and when we take the square root we get

$$(\nabla\alpha \times \nabla\beta)_x = \imath\left(\partial_t\alpha\partial_x\beta - \partial_t\beta\partial_x\alpha\right)$$

5

Similar arguments give us the y- and z-components of $\nabla\alpha \times \nabla\beta$ as

$$(\nabla\alpha \times \nabla\beta)_y = \imath \left(\partial_t\alpha\partial_y\beta - \partial_t\beta\partial_y\alpha\right)$$

$$(\nabla\alpha \times \nabla\beta)_z = \imath \left(\partial_t\alpha\partial_z\beta - \partial_t\beta\partial_z\alpha\right)$$

and we have established (5). We now consider the following operations on $\nabla\alpha \times \nabla\beta$

$$\nabla \times (\nabla\alpha \times \nabla\beta) \qquad \text{and} \qquad \nabla \cdot (\nabla\alpha \times \nabla\beta) \tag{7}$$

We will first consider

$$\nabla \times (\nabla\alpha \times \nabla\beta) = \nabla \times \left(\imath \left(\partial_t\alpha\nabla\beta - \partial_t\beta\nabla\alpha\right)\right) = \imath \left[\nabla \times (\partial_t\alpha\nabla\beta) - \nabla \times (\partial_t\beta\nabla\alpha)\right]$$

$$= \imath \left[\nabla\partial_t\alpha \times \nabla\beta + \partial_t\alpha\cancel{\nabla \times \nabla\beta} - (\nabla\partial_t\beta \times \nabla\alpha + \partial_t\beta\cancel{\nabla \times \nabla\alpha})\right]$$

$$= \imath \left[\nabla\partial_t\alpha \times \nabla\beta - \nabla\partial_t\beta \times \nabla\alpha\right] = \imath \left[\nabla\partial_t\alpha \times \nabla\beta + \nabla\alpha \times \nabla\partial_t\beta\right]$$

$$= \imath\,\partial_t \left[\nabla\alpha \times \nabla\beta\right]$$

and we also find that

$$\nabla \cdot (\nabla\alpha \times \nabla\beta) = \nabla\beta \cdot (\cancel{\nabla \times \nabla\alpha}) - \nabla\alpha \cdot (\cancel{\nabla \times \nabla\beta}) = 0$$

From this we see that $\nabla\alpha \times \nabla\beta$ and the electromagnetic field, $\mathbf{F}$, possess the same properties (4) and we define

$$\mathbf{F} = \nabla\alpha \times \nabla\beta \tag{8}$$

It should be noted that for all α, β satisfying the above properties, we can obtain a field $\mathbf{F}$, but the converse may not be true; namely that for a given $\mathbf{F}$, it may not be possible to determine functions α, β satisfying the same properties. As we will be working the problem from one direction (i.e. choosing suitable α and β), we will leave that question open. Using

this definition, we can ascertain another property of $\mathbf{F}$. Computing $\mathbf{F} \cdot \mathbf{F}$ we determine that

$$
\begin{aligned}
\mathbf{F} \cdot \mathbf{F} &= (\nabla\alpha \times \nabla\beta) \cdot \left[\imath \left(\partial_t \alpha \nabla\beta - \partial_t \beta \nabla\alpha \right) \right] \\
&= \imath \left[(\nabla\alpha \times \nabla\beta) \cdot \partial_t \alpha \nabla\beta - (\nabla\alpha \times \nabla\beta) \cdot \partial_t \beta \nabla\alpha \right] \\
&= \imath \left[\partial_t \alpha \left(\nabla\beta \times \nabla\beta \right) \cdot \nabla\alpha - \partial_t \beta \left(\nabla\alpha \times \nabla\alpha \right) \cdot \nabla\beta \right] = 0
\end{aligned}
$$

From the previous definition of $\mathbf{F}$, in (3), we have that

$$
\mathbf{F} \cdot \mathbf{F} = (\mathbf{E} + \imath\mathbf{B}) \cdot (\mathbf{E} + \imath\mathbf{B}) = \mathbf{E} \cdot \mathbf{E} - \mathbf{B} \cdot \mathbf{B} + 2\,\imath \, (\mathbf{E} \cdot \mathbf{B})
$$

and from above, we know that this term must be 0 in both its real and imaginary parts. We conclude that

$$
\mathbf{E} \cdot \mathbf{E} - \mathbf{B} \cdot \mathbf{B} = 0 \quad \Rightarrow \quad \mathbf{E} \cdot \mathbf{E} = \mathbf{B} \cdot \mathbf{B} \qquad \text{and} \qquad \mathbf{E} \cdot \mathbf{B} = 0 \tag{9}
$$

A field with these properties is referred to as a null field. A null field is a field in which the electric and magnetic fields are mutually orthogonal and have the same magnitude (in geometrized units) in all reference frames. For a field that is not a null field, a reference frame can be found in which either the electric or magnetic field vanishes [11]. This construction guarantees that the field is null for all time. When a pair of functions (α, β) has been found to satisfy these conditions, we can construct an entire family of null fields. The individual members of this family differ in their electric and magnetic components, but their Poynting fields are all the same. To see this, we let

$$
f(\alpha, \beta) \qquad \text{and} \qquad g(\alpha, \beta)
$$

be two arbitrary holomorphic (or analytic) complex scalar functions of α and β. We define

$$h(\alpha, \beta) = \partial_\alpha f \partial_\beta g - \partial_\beta f \partial_\alpha g = \frac{\partial(f, g)}{\partial(\alpha, \beta)} \tag{10}$$

Now we consider

$$
\nabla f(\alpha, \beta) \times \nabla g(\alpha, \beta) = \begin{vmatrix} \hat{\mathbf{i}} & \hat{\mathbf{j}} & \hat{\mathbf{k}} \\ \partial_\alpha f \partial_x \alpha + \partial_\beta f \partial_x \beta & \partial_\alpha f \partial_y \alpha + \partial_\beta f \partial_y \beta & \partial_\alpha f \partial_z \alpha + \partial_\beta f \partial_z \beta \\ \partial_\alpha g \partial_x \alpha + \partial_\beta g \partial_x \beta & \partial_\alpha g \partial_y \alpha + \partial_\beta g \partial_y \beta & \partial_\alpha g \partial_z \alpha + \partial_\beta g \partial_z \beta \end{vmatrix}
$$

$$
= \frac{\partial(f, g)}{\partial(\alpha, \beta)} \left[\frac{\partial(\alpha, \beta)}{\partial(y, z)} \hat{\mathbf{i}} - \frac{\partial(\alpha, \beta)}{\partial(x, z)} \hat{\mathbf{j}} + \frac{\partial(\alpha, \beta)}{\partial(x, y)} \hat{\mathbf{k}} \right]
$$

$$
= h(\alpha, \beta) \left(\nabla \alpha \times \nabla \beta \right)
$$

Thus we have generated an infinite family of null fields, determined by α and β, that satisfy Maxwell's equations in free space. For fixed α and β, different choices of f and g give different members of the family, but α and β determine this family.

$$\nabla f(\alpha, \beta) \times \nabla g(\alpha, \beta) = h(\alpha, \beta) \left(\nabla \alpha \times \nabla \beta \right) \tag{11}$$

In calculating the normalized Poynting field, we find that

$$\mathbf{E} \times \mathbf{B} = (\mathbf{F} - \imath \mathbf{B}) \times \mathbf{B} = \mathbf{F} \times \mathbf{B} - \imath \cancel{\mathbf{B} \times \mathbf{B}} = \mathbf{F} \times \mathbf{B}$$

and

$$\mathbf{E} \times \mathbf{B} = \mathbf{E} \times \left(\frac{1}{\imath}(\mathbf{F} - \mathbf{E}) \right) = -\imath \left(\mathbf{E} \times \mathbf{F} - \cancel{\mathbf{E} \times \mathbf{E}} \right) = \imath (\mathbf{F} \times \mathbf{E})$$

$$\Rightarrow \quad \mathbf{E} \times \mathbf{B} = \frac{1}{2} \left(\mathbf{F} \times \mathbf{B} + \imath \, \mathbf{F} \times \mathbf{E} \right) = \frac{\imath}{2} \left(\mathbf{F} \times (-\imath \mathbf{B} + \mathbf{E}) \right)$$

$$= \frac{\imath}{2} (\mathbf{F} \times \mathbf{F}^*)$$

where the $*$ superscript denotes complex conjugation. Furthermore, we also have that

$$|\mathbf{E} \times \mathbf{B}| = \sqrt{(\mathbf{E} \times \mathbf{B}) \cdot (\mathbf{E} \times \mathbf{B})} = \sqrt{(\mathbf{E} \cdot \mathbf{E})(\mathbf{B} \cdot \mathbf{B}) - (\mathbf{E} \cdot \mathbf{B})^2} = \mathbf{E} \cdot \mathbf{E} = \mathbf{B} \cdot \mathbf{B}$$

where we have used (9). Now consider

$$
\begin{aligned}
\mathbf{F} \cdot \mathbf{F}^* &= (\mathbf{E} + \imath \, \mathbf{B}) \cdot (\mathbf{E} - \imath \, \mathbf{B}) \\
&= \mathbf{E} \cdot \mathbf{E} + \mathbf{B} \cdot \mathbf{B} + \imath \, \mathbf{E} \cdot \mathbf{B} - \imath \, \mathbf{E} \cdot \mathbf{B} \\
&= \mathbf{E} \cdot \mathbf{E} + \mathbf{B} \cdot \mathbf{B} = 2\mathbf{E} \cdot \mathbf{E} = 2\mathbf{B} \cdot \mathbf{B} \\
&= 2|\mathbf{E} \times \mathbf{B}|
\end{aligned}
$$

So, now we have that the normalized Poynting field can be expressed as

$$
\begin{aligned}
\frac{\mathbf{E} \times \mathbf{B}}{|\mathbf{E} \times \mathbf{B}|} &= \imath \left(\frac{\mathbf{F} \times \mathbf{F}^*}{\mathbf{F} \cdot \mathbf{F}^*} \right) = \imath \frac{|h(\alpha, \beta)|^2}{|h(\alpha, \beta)|^2} \left(\frac{(\nabla \alpha \times \nabla \beta) \times (\nabla \alpha^* \times \nabla \beta^*)}{(\nabla \alpha \times \nabla \beta) \cdot (\nabla \alpha^* \times \nabla \beta^*)} \right) \\
&= \imath \frac{(\nabla \alpha \times \nabla \beta) \times (\nabla \alpha^* \times \nabla \beta^*)}{(\nabla \alpha \times \nabla \beta) \cdot (\nabla \alpha^* \times \nabla \beta^*)}
\end{aligned}
\tag{12}
$$

and we readily see that the normalized Poynting field for all members of the family depend only on α and β.

2.3 Remarks

From this we see that for each pair, $(\alpha(x, y, z, t), \beta(x, y, z, t))$, of appropriately chosen functions, the normalized Poynting field is the same for all fields within the family, regardless of the arbitrary functions $f(\alpha, \beta)$ and $g(\alpha, \beta)$.

The following section will illustrate a specific example.

3 Elliptically Polarized Plane Wave

3.1 Parameters

With the appropriate choice of α, β, f and g, we are able to construct the readily recognizable elliptically polarized plane wave. Let

$$\alpha(x, y, z, t) = z - t \qquad \beta(x, y, z, t) = x + \imath y \qquad f(\alpha, \beta) = e^{\imath\alpha} \qquad g(\alpha, \beta) = \beta$$

and we see that

$$(\nabla\alpha)^2 = 1^2 = 1 \qquad \left(\frac{\partial\alpha}{\partial t}\right)^2 = (-1)^2 = 1$$

$$(\nabla\beta)^2 = 1^2 + \imath^2 = 0 \qquad \left(\frac{\partial\beta}{\partial t}\right)^2 = 0$$

$$\nabla\alpha \cdot \nabla\beta = (0, 0, 1) \cdot (1, \imath, 0) = 0 \qquad \partial_t\alpha\,\partial_t\beta = 1 \cdot 0 = 0$$

so α and β satisfy (6). Using the construction of the previous section, we see that

$$\mathbf{F} = \nabla f(\alpha, \beta) \times \nabla g(\alpha, \beta) = \nabla\left(e^{\imath(z-t)}\right) \times \nabla\left(x + \imath y\right)$$

$$= \begin{vmatrix} \hat{\mathbf{i}} & \hat{\mathbf{j}} & \hat{\mathbf{k}} \\ 0 & 0 & \imath e^{\imath(z-t)} \\ 1 & \imath & 0 \end{vmatrix} = \hat{\mathbf{i}}\left(0 + e^{\imath(z-t)}\right) - \hat{\mathbf{j}}\left(0 - \imath e^{\imath(z-t)}\right) + \hat{\mathbf{k}}\left(0 - 0\right)$$

$$= e^{\imath(z-t)}\left(\hat{\mathbf{i}} + \imath\hat{\mathbf{j}}\right) = \mathbf{E} + \imath\mathbf{B}$$

so we obtain:

$$\mathbf{E} = \cos(z - t)\hat{\mathbf{i}} - \sin(z - t)\hat{\mathbf{j}} \qquad \text{and} \qquad \mathbf{B} = \sin(z - t)\hat{\mathbf{i}} + \cos(z - t)\hat{\mathbf{j}} \tag{13}$$

Furthermore, we are able to calculate the normalized Poynting field as well, using (12),

we get that

$$\mathbf{F} \times \mathbf{F}^* = \begin{vmatrix} \hat{\mathbf{i}} & \hat{\mathbf{j}} & \hat{\mathbf{k}} \\ e^{i(z-t)} & i e^{i(z-t)} & 0 \\ e^{-i(z-t)} & -i e^{-i(z-t)} & 0 \end{vmatrix} = \hat{\mathbf{k}} \left(-i - i \right) = -2i\hat{\mathbf{k}}$$

and

$$\mathbf{F} \cdot \mathbf{F}^* = e^{(z-t)(i-i)} + i(-i)e^{(z-t)(i-i)} = 2$$

and we get that

$$i \left(\frac{\mathbf{F} \times \mathbf{F}^*}{\mathbf{F} \cdot \mathbf{F}^*} \right) = i \left(\frac{-2i\hat{\mathbf{k}}}{2} \right) = \hat{\mathbf{k}}$$

which is what we would expect.

3.2   Verifications

With this simple example, we will verify (11). To determine the function h defined by f and g we obtain:

$$h(\alpha, \beta) = \frac{\partial(f, g)}{\partial(\alpha, \beta)} = i e^{i\alpha}$$

and

$$\nabla \alpha \times \nabla \beta = \begin{vmatrix} \hat{\mathbf{i}} & \hat{\mathbf{j}} & \hat{\mathbf{k}} \\ 0 & 0 & 1 \\ 1 & i & 0 \end{vmatrix} = -i\hat{\mathbf{i}} + \hat{\mathbf{j}}$$

so

$$h(\alpha, \beta) \left(\nabla \alpha \times \nabla \beta \right) = i e^{i(z-t)} \left(i\hat{\mathbf{i}} + \hat{\mathbf{j}} \right) = e^{i(z-t)} \left(\hat{\mathbf{i}} + i\hat{\mathbf{j}} \right) = \mathbf{F}$$

and the construction is verified.

3.3 Remarks

We have constructed a family of solutions where all members of this family have the same underlying structure attached to their Poynting fields. In the literature this tie that all members of the family share is called a *congruence*, for the case of the Hopfion solution, this is referred to as the *Robinson congruence* [16].

The following section provides some background on the torus as this structure will be prevalent in subsequent discussions.

4   The Torus

This section will give some background information about tori. The surface of a torus is important in that it is one of the simplest non-trivial surfaces in the study of topology. The formal, topological definition of a torus is the product of circles.

$$T^n = \underbrace{S^1 \times S^1 \times \cdots \times S^1}_{n \text{ copies}}$$

where S^1 is the unit circle. We will confine our observations to the 2-torus, $T^2 = S^1 \times S^1$. The surface of the torus can be mapped continuously to a finite plane with the sides identified as in Figure 1
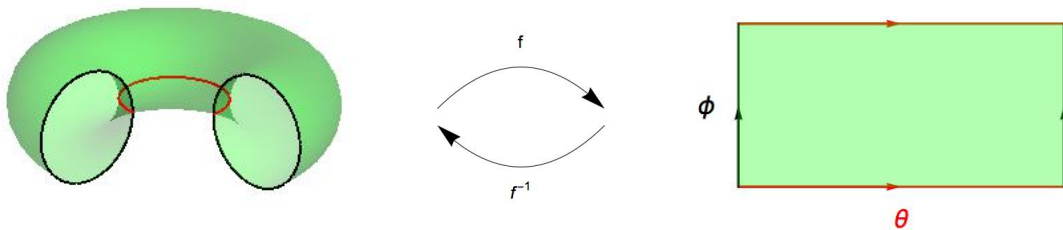
Figure 1: The 2-torus and the plane are topologically equivalent. The mapping f takes the torus to the plane, and f^{-1} takes the plane to the torus

It is easy enough to understand and observe that such a continuous mapping is possible. Obtaining an explicit form for f is not entirely obvious. We will only concern ourselves with the reverse map f^{-1}. We define the axes of the finite plane to be the variables (θ, ϕ), we see that

$$f^{-1} : \{0, 2\pi\} \times \{0, 2\pi\} \to T^2 \subset \mathbb{R}^3$$

and explicitly

$$f^{-1}(\theta, \phi) = \big((r + (1-r)\cos\theta)\cos\phi, (r + (1-r)\cos\theta)\sin\phi, (1-r)\sin\theta \big)$$

maps to the torus with r as the radius from the center of the torus to the center of the tube

13

and $1 - r$ as the radius of the tube. Of course, there are an infinite number of tori that can be generated in this way. This parameterization will be useful when we discuss the Hopf fibration in the following sections. As r ranges from $1 \to \infty$ we obtain a series of nested tori as in Figure 2
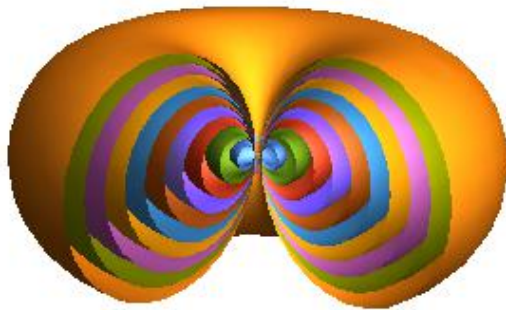
Figure 2: Nested tori. As r increases from $1 \to \infty$, the center of the tube extends out to infinity and the hole shrinks

It should be noted that with this parameterization, we need to identify two degenerate 'tori'. They occur when $r = 1$ and $r = \infty$. The first is simply the unit circle lying in the xy-plane (an infinitely thin torus). The second is the z-axis (torus of infinite radius), this 'torus' must be identified to include the limit point at infinity.

The map f from the torus to the plane is substantially trickier, due to the fact that the edges are identified. This requires that the forward map be defined in a piecewise manner.

5 The Hopfion Solution

5.1 Introduction

There is an interesting structure, first discovered and studied by Heinz Hopf [5] in 1931, that has been recently rediscovered and found to have applications in various fields. This structure helps to illustrate some of the properties of the 3-sphere, S^3, that would otherwise be unknown. A *fibration* is a continuous map $\pi : X \to Y$ between topological spaces that preserve homotopies. This means that a homotopy from X to Y is still a homotopy under the map π. These types of maps are important because they reveal characteristics of unknown or unfamiliar spaces.

  As this is a physics thesis and some the objects and concepts may be unfamiliar, I will provide some definitions [9]. A topological space is a set of points together with a definition of open subsets. This definition provides a notion of which points in the set are 'close' to each other. We used quotes around close because this is different from a metric space in that we cannot assign an explicit number to the distance between points. We are only able to say that two points are either in the same neighborhood or they are not. A homotopy is a continous collection of continous functions $F(x,t) : X \times I \to Y$, where I is the unit interval $[0,1]$, such that $F(x,0) = f_1(x)$ and $F(x,1) = f_2(x)$ and $F(x,t)$ is continuous in both x and t. Fundamentally this says that $f_1(x)$ can be continously deformed into $f_2(x)$ in both topological spaces X and Y, where f_1 and f_2 are themselves continuous in X and they are said to be homotopic. A familiar example of a homotopy is the aging process. An infant, f_1, and an elderly person, f_2, are equivalent topologically (barring any sort of surgery such as an apendectomy) and the homotopy is the path $F(x,t)$ the body takes as time goes by. This process is continuous and the topological shapes are equivalent at each point in time. So a fibration is a map that preserve the homotopic relationship between f_1 and f_2.

5.2 The Hopf Fibration

The Hopf fibration is a mapping $h : S^3 \to S^2$ defined by the relations [12]

$$h(a, b, c, d) = \left(a^2 + b^2 - c^2 - d^2, 2(ad + bc), 2(bd - ac)\right) \tag{14}$$

where $a^2 + b^2 + c^2 + d^2 = 1$, since the domain is the 3-sphere. It should be noted that the range of this map is the 2-sphere. To show this, we find the magnitude of the points in the range by computing

$$\begin{aligned}
\sqrt{h \cdot h} &= \left[\left(a^2 + b^2 - c^2 - d^2\right)^2 + 4\left(ad + bc\right)^2 + 4\left(bd - ac\right)^2\right]^{1/2} \\
&= \left[a^4 + b^2 + c^2 + d^2 + 2a^2b^2 - 2a^2c^2 - 2a^2d^2 - 2b^2c^2 - 2b^2d^2 + 2c^2d^2 \right. \\
&\quad \left. + 4a^2d^2 + 4b^2c^2 + 8abcd + 4b^2d^2 + 4a^2c^2 - 8abcd\right]^{1/2} \\
&= \left[\left(a^2 + b^2 + c^2 + d^2\right)^2\right]^{1/2} = a^2 + b^2 + c^2 + d^2 = 1
\end{aligned}$$

Thus, the range is indeed the 2-sphere. We can alternatively define this map using complex numbers. We first identify the 3-sphere with $\mathbb{C}^2 = \mathbb{C} \times \mathbb{C}$ and the 2-sphere with $\mathbb{C} \times \mathbb{R}$

$$S^3 = \left\{(z_0, z_1) \in \mathbb{C} \times \mathbb{C} \,\middle|\, |z_0|^2 + |z_1|^2 = 1\right\} \qquad \text{and}$$
$$S^2 = \left\{(z, x) \in \mathbb{C} \times \mathbb{R} \,\middle|\, |z|^2 + x^2 = 1\right\}$$

We can then define the Hopf map using this notation

$$h_{\mathbb{C}}(z_0, z_1) = \left(2z_0\bar{z}_1, |z_0|^2 - |z_1|^2\right) \tag{15}$$

16

and we note that the first term is complex (in general) and the second term is real. We can double check that this mapping lies on the 2-sphere.

$$|h_{\mathbb{C}}(z_0, z_1)| = 4z_0\bar{z}_1\bar{z}_0 z_1 + |z_0|^4 - 2|z_0|^2|z_1|^2 + |z_1|^4$$
$$= |z_0|^4 + 2|z_0|^2|z_1|^2 + |z_1|^4 = \left(|z_0|^2 + |z_1|^2\right)^2 = 1,$$

and indeed it does. This formulation coincides with the previous one when we let $z_0 = a + \imath b$ and $z_1 = c + \imath d$.

As the space S^3 is 'bigger' than the space S^2, it seems obvious that this map is surjective (i.e. multiple points in the domain may map to the same point in the range). Consider a point in S^3 such that $(w_0, w_1) = (\lambda z_0, \lambda z_1)$. In this instance, we have that

$$h_{\mathbb{C}}(w_0, w_1) = \left(2\lambda z_0\bar{\lambda}\bar{z}_1, |\lambda|^2 \left(|z_0|^2 + |z_1|^2\right)\right) = |\lambda|^2 h_{\mathbb{C}}(z_0, z_1)$$

and the two points in S^3 map to the same point in S^2, as long as $|\lambda|^2 = 1$. Then we can say that $\lambda = e^{\imath\xi}$, where ξ ranges from 0 to 2π. This allows us to observe that the preimage of a point on S^2 is a great circle on S^3, passing through the point (z_0, z_1). These circles are the fibers (the set of points that map to the same point) that make up the fibration and they can be parameterized explicitly as follows:

$$\begin{aligned} z_0 &= e^{\imath(\xi + \frac{\phi}{2})} \sin\left(\frac{\theta}{2}\right) \\ z_1 &= e^{\imath(\xi - \frac{\phi}{2})} \cos\left(\frac{\theta}{2}\right) \end{aligned} \tag{16}$$

To see this, we let $z_0 = r_0 e^{\xi_0}$ and $z_1 = r_1 e^{\xi_1}$. Then we have that

$$h_{\mathbb{C}}(z_0, z_1) = \left(2z_0\bar{z}_1, |z_0|^2 - |z_1|^2\right) = \left(2r_0 r_1 e^{\imath(\xi_0 - \xi_1)}, r_0^2 - r_1^2\right),$$

and this must map to a point on S^2 so we have the relations

$$x = \sin\theta\cos\phi = \text{Re}\left[2r_0 r_1 e^{\imath(\xi_0 - \xi_1)}\right] = 2r_0 r_1 \cos(\xi_0 - \xi_1)$$

$$y = \sin\theta\sin\phi = \text{Im}\left[2r_0 r_1 e^{\imath(\xi_0 - \xi_1)}\right] = 2r_0 r_1 \sin(\xi_0 - \xi_1)$$

$$z = \cos\theta = r_0^2 - r_1^2$$

and we see immediately that $\phi = \xi_0 - \xi_1$, and, after a little algebra we find that:

$$\left(r_0^2 - r_1^2\right) + \left(r_0^2 + r_1^2\right) = 1 + \cos\theta$$

$$r_0^2 = \frac{1 + \cos\theta}{2} = \cos^2\left(\frac{\theta}{2}\right)$$

$$\Rightarrow \qquad r_0 = \cos\left(\frac{\theta}{2}\right)$$

Similarly we obtain that $r_1 = \sin(\theta/2)$ so now we have:

$$z_0 = \cos\left(\frac{\theta}{2}\right)e^{\imath\xi_0} \qquad \text{and} \qquad z_1 = \sin\left(\frac{\theta}{2}\right)e^{\imath(\xi_0 - \phi)} \tag{17}$$

Now we define $\lambda = e^{\imath\left(\xi - \xi_0 + \frac{\phi}{2}\right)}$, where ξ ranges from 0 to 2π, and we obtain:

$$w_0 = \lambda z_0 = \cos\left(\frac{\theta}{2}\right)e^{\imath\left(\xi + \frac{\phi}{2}\right)} \qquad \text{and} \qquad w_1 = \lambda z_1 = \sin\left(\frac{\theta}{2}\right)e^{\imath\left(\xi - \frac{\phi}{2}\right)} \tag{18}$$

which is what we were trying to demonstrate. This is, in essence, the reverse map $h_{\mathbb{C}}^{-1}(w, x)$, since we took a point on S^2 and found its preimage on S^3. Now we need to figure out how to 'see' what's going on.

Stereographic Projection

The 3-sphere, S^3, is an entirely abstract entity. It is a surface embedded in $\mathbb{R}^4$, which is an unimaginable space. To understand its relation to $\mathbb{R}^3$, we utilized the notion of stereographic projection. We first use this process for S^2 and then we make the generalization to higher

dimensions.

We embed S^2 in $\mathbb{R}^3$ and consider lines drawn from the top of the sphere $(0, 0, 1)$ to any other point on the sphere and see where that line intersects the xy-plane, as in Figure 3. This is often referred to as the Riemann sphere.
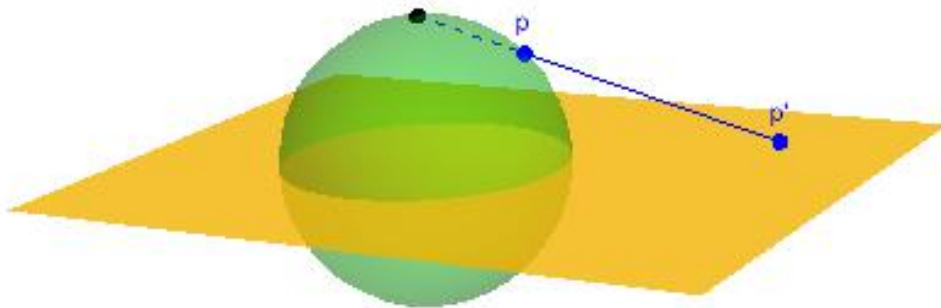
Figure 3: The Riemann Sphere. Stereographic projection of the point p in S^2 to the point p' on the xy-plane

This map (we'll call it s_2), takes a point on S^2 and maps it to a point in $\mathbb{R}^2$ and it has the explicit form:

$$s_2(x, y, z) = \left(\frac{x}{1 - z}, \frac{y}{1 - z} \right) \tag{19}$$

where, of course, we require that $x^2 + y^2 + z^2 = 1$. We see here that the surface of the 2-sphere is a 'curved' version of $\mathbb{R}^2$. We can generalize this to higher dimensions and we will find that the 3-sphere is in fact a 'curved' version of $\mathbb{R}^3$. We are only interested in the map $s_3 : S^3 \to \mathbb{R}^3$ and it is given by

$$s_3(x, y, z, w) = \left(\frac{x}{1 - w}, \frac{y}{1 - w}, \frac{z}{1 - w} \right) \tag{20}$$

It should be noted that the point that we project from is not well defined by these relations.

This can be rectified by eliminating that point from the domain spaces and we state:

$$s_2 : S^2 \setminus \{0, 0, 1\} \to \mathbb{R}^2 \quad \text{and} \quad s_3 : S^3 \setminus \{0, 0, 0, 1\} \to \mathbb{R}^3$$

this map is, in fact, conformal, in that it preserves angles and shapes. This property applies to circles as well. Therefore, circles in S^3 (preimages of the Hopf map) map to circles in $\mathbb{R}^3$ via stereographic projection. The remarkable property of the Hopf Fibration can now be determined. When we take the stereographic projection of the preimage of the Hopf map from (18), we find that

$$s_3(w_0, w_1) = \frac{1}{1 - \sin\left(\frac{\theta}{2}\right)\sin\left(\xi - \frac{\phi}{2}\right)}$$
$$\left(\cos\left(\frac{\theta}{2}\right)\cos\left(\xi + \frac{\phi}{2}\right), \cos\left(\frac{\theta}{2}\right)\sin\left(\xi + \frac{\phi}{2}\right), \sin\left(\frac{\theta}{2}\right)\cos\left(\xi - \frac{\phi}{2}\right) \right) \tag{21}$$

For any two points on S^2, the corresponding circles they map to in $\mathbb{R}^3$ will always be linked together, as in Figure 4. Another interesting property occurs when considering the image of a specific latitude of the 2-sphere. These points evidently map to a torus in $\mathbb{R}^3$, as in Figure 5, the structure of the Hopf fibration is apparent in Figure 6.

Furthermore, it is quite simple to deterimine the inverse of stereographic projection. This map takes a point in $\mathbb{R}^3$ and gives the preimage on S^3 of that point. It is given by

$$s_3^{-1}(x, y, z) = \frac{1}{x^2 + y^2 + z^2 + 1} \left(2x, 2y, 2z, x^2 + y^2 + z^2 - 1 \right) \tag{22}$$

$$= (a, b, c, d) \in S^3$$

5.3 Parameters

It turns out that a solution to Maxwell's equations can be constructed such that the electric, magnetic, and Poynting fields each, independently, have the structure of the Hopf Fibration. The individual field lines of each of these fields are closed loops, and any two of these loops
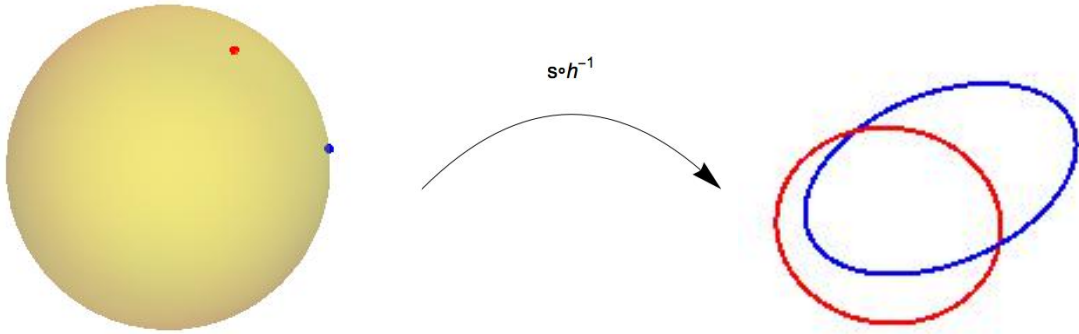
Figure 4: The fibers of the Hopf map are linked circles. The mapping $s \circ h^{-1}$ takes the points on the 2-sphere and maps them to circles in $\mathbb{R}^3$. Any distinct points map to circles that are linked exactly once.
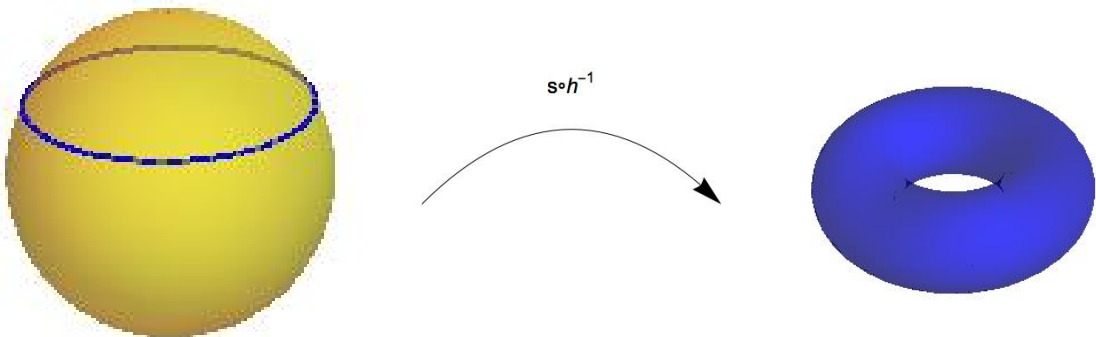
Figure 5: Latitudes produce tori. The Hopf map takes the points on a specific latitude to a torus, T^2, in $\mathbb{R}^3$

are linked exactly once. Returning to Bateman's construction we define the parameters for such a solution. They turn out to be [3,8]

$$\alpha = -\frac{d}{b} \qquad \beta = -\frac{\imath a}{2b} \qquad f = \frac{1}{\alpha^2} \qquad g = \beta \tag{23}$$

21
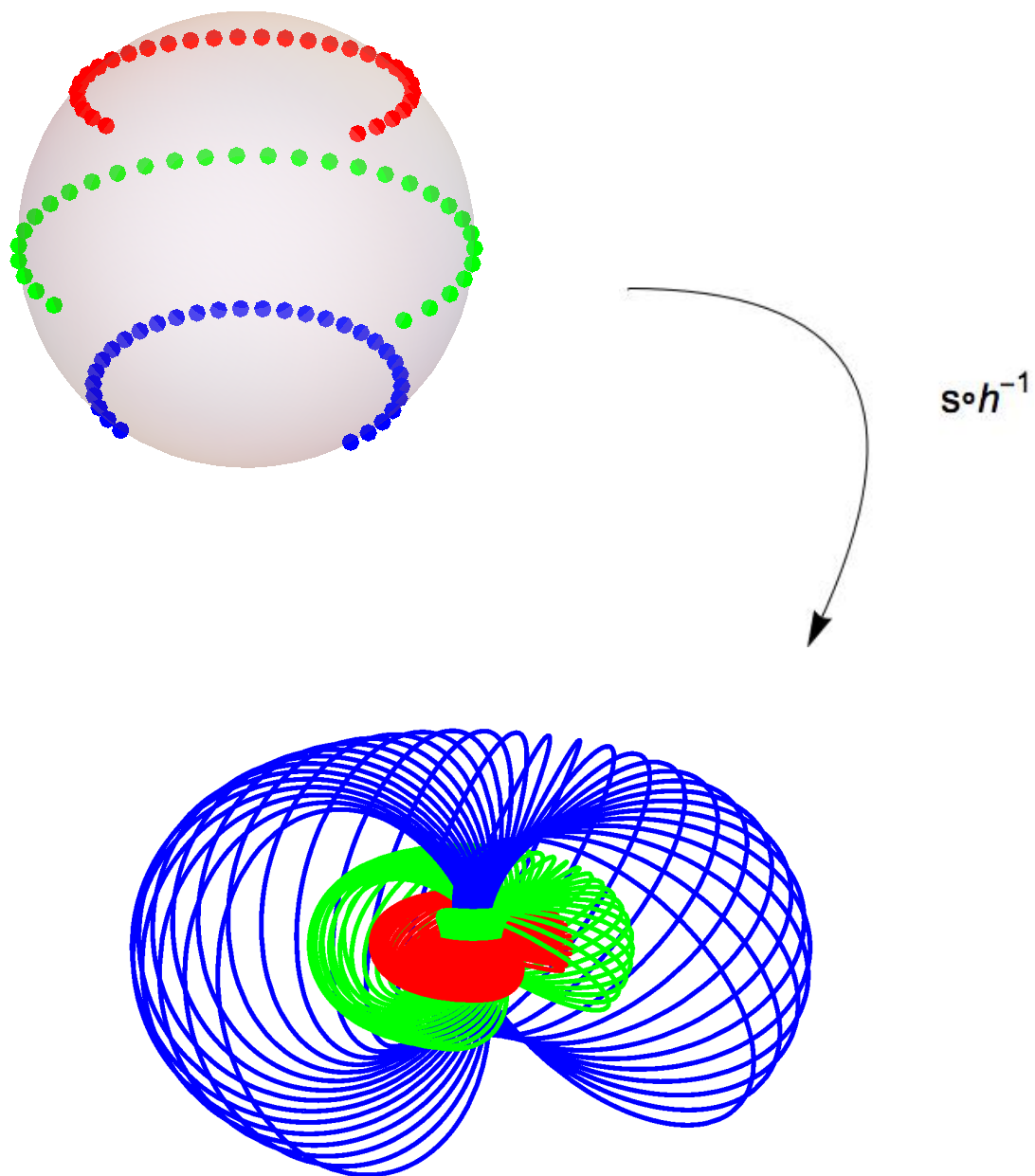
Figure 6: The Hopf fibration. Every point on the 2-sphere produces a fiber that is a circle, any two of which are linked. Points that share a latitude produce a torus and the tori produced at each latitude are nested inside one another.

where

$$a = x - \imath y \qquad b = t - \imath - z \qquad d = r^2 - (t - \imath)^2, \tag{24}$$

and now we determine

$$\nabla \alpha = (\partial_x \alpha, \partial_y \alpha, \partial_z \alpha) \qquad \text{and} \qquad \nabla \beta = (\partial_x \beta, \partial_y \beta, \partial_z \beta)$$

with

$$\partial_x \alpha = -\frac{b \, \partial_x d - d \, \partial_x b}{b^2} = -\frac{2bx}{b^2} = -\frac{2x}{b}$$

similarly

$$\partial_y \alpha = -\frac{b \, \partial_y d - d \, \partial_y b}{b^2} = -\frac{2by}{b^2} = -\frac{2y}{b}$$

and

$$\partial_z \alpha = -\frac{b \, \partial_z d - d \, \partial_z b}{b^2} = -\frac{2bz + d}{b^2}$$

so, we have that

$$\nabla \alpha = -\frac{1}{b^2} \left(2bx, 2by, 2bz + d\right) \tag{25}$$

and

$$\partial_x \beta = -\frac{\imath}{2} \frac{b \, \partial_x a - a \, \partial_x b}{b^2} = -\frac{\imath}{2} \frac{b}{b^2} = -\frac{\imath}{2b}$$

$$\partial_y \beta = -\frac{\imath}{2} \frac{b \, \partial_y a - a \, \partial_y b}{b^2} = -\frac{\imath}{2} \frac{-\imath b}{b^2} = -\frac{1}{2b}$$

$$\partial_z \beta = -\frac{\imath}{2} \frac{b \, \partial_z a - a \, \partial_z b}{b^2} = -\frac{\imath}{2} \frac{a}{b^2} = -\frac{\imath a}{2b^2}$$

so

$$\nabla \beta = -\frac{1}{2b^2} \left(\imath b, b, \imath a\right) \tag{26}$$

23

now we are able to determine

$$\nabla\alpha \times \nabla\beta = \begin{vmatrix} \hat{\mathbf{i}} & \hat{\mathbf{j}} & \hat{\mathbf{k}} \\ \partial_x\alpha & \partial_y\alpha & \partial_z\alpha \\ \partial_x\beta & \partial_y\beta & \partial_z\beta \end{vmatrix} = \frac{1}{2b^4} \begin{vmatrix} \hat{\mathbf{i}} & \hat{\mathbf{j}} & \hat{\mathbf{k}} \\ 2bx & 2by & 2bz+d \\ \imath b & b & \imath a \end{vmatrix}$$

$$= \frac{1}{2b^4} \left[\hat{\mathbf{i}} \left(2\imath aby - 2b^2z - bd \right) - \hat{\mathbf{j}} \left(2\imath abx - 2\imath b^2z - \imath bd \right) + \hat{\mathbf{k}} \left(2b^2x - 2\imath b^2y \right) \right]$$

$$= \frac{1}{2b^3} \left[\hat{\mathbf{i}} \left(2\imath ay - 2bz - d \right) - \hat{\mathbf{j}} \left(2\imath ax - 2\imath bz - \imath d \right) + \hat{\mathbf{k}} \left(2bx - 2\imath by \right) \right]$$

$$= \frac{1}{2b^3} \left[\left(b^2 - a^2 \right) \hat{\mathbf{i}} + \imath \left(a^2 + b^2 \right) \hat{\mathbf{j}} + 2ab\,\hat{\mathbf{k}} \right]$$

and we also have from (10) that

$$h(\alpha, \beta) = \partial_\alpha f \partial_\beta g - \partial_\beta f \partial_\alpha g = -\frac{2}{\alpha^3} = \frac{2b^3}{d^3}$$

and we determine that

$$\mathbf{F} = h(\alpha, \beta) \left(\nabla\alpha \times \nabla\beta \right) = \frac{1}{d^3} \left(b^2 - a^2, \imath \left(a^2 + b^2 \right), 2ab \right)$$

Decomposing this expression into its real and imaginary components to determine the electric and magnetic fields, we find that at time $t = 0$

$$\mathbf{E} = \frac{1}{(1 + x^2 + y^2 + z^2)^3} \left(-1 - x^2 + y^2 + z^2, -2(xy - z), -2(y + xz) \right) \tag{27}$$

and

$$\mathbf{B} = \frac{1}{(1 + x^2 + y^2 + z^2)^3} \left(2(xy + z), 1 - x^2 + y^2 - z^2, -2(x - yz) \right) \tag{28}$$

The normalized Poynting field is determined using (12)

$$\frac{\mathbf{E} \times \mathbf{B}}{|\mathbf{E} \times \mathbf{B}|} = \imath \left(\frac{\mathbf{F} \times \mathbf{F}^*}{\mathbf{F} \cdot \mathbf{F}^*} \right),$$

and we find that

$$\mathbf{F} \cdot \mathbf{F}^* = \frac{1}{|d|^6} \left[\left(b^2 - a^2 \right) \left(\bar{b}^2 - \bar{a}^2 \right) + \left(a^2 + b^2 \right) \left(\bar{a}^2 + \bar{b}^2 \right) + 4|a|^2|b|^2 \right]$$

$$= \frac{1}{|d|^6} \left(|b|^4 + |a|^4 - a^2\bar{b}^2 - \bar{a}^2 b^2 + |a|^4 + |b|^4 + a^2\bar{b}^2 + \bar{a}^2 b^2 + 4|a|^2|b|^2 \right)$$

$$= \frac{2}{|d|^6} \left(|a|^4 + 2|a|^2|b|^2 + |b|^2 \right) = \frac{2}{|d|^6} \left(|a|^2 + |b|^2 \right)^2$$

and

$$\mathbf{F} \times \mathbf{F}^* = \frac{1}{|d|^6} \begin{vmatrix} \hat{\mathbf{i}} & \hat{\mathbf{j}} & \hat{\mathbf{k}} \\ b^2 - a^2 & \imath \left(a^2 + b^2 \right) & 2ab \\ \bar{b}^2 - \bar{a}^2 & -\imath \left(\bar{a}^2 + \bar{b}^2 \right) & 2\bar{a}\bar{b} \end{vmatrix}$$

Determining the components we obtain:

$$\begin{aligned}
(\mathbf{F} \times \mathbf{F}^*)_{\hat{\mathbf{i}}} &= \left[2\imath\bar{a}\bar{b} \left(a^2 + b^2 \right) + 2\imath ab \left(\bar{a}^2 + \bar{b}^2 \right) \right] \\
&= 2\imath \left[\bar{b}a|a|^2 + \bar{a}b|b|^2 + b\bar{a}|a|^2 + a\bar{b}|b|^2 \right] \\
&= 2\imath \left[a\bar{b} \left(|a|^2 + |b|^2 \right) + \bar{a}b \left(|a|^2 + |b|^2 \right) \right] \\
&= 2\imath \left(a\bar{b} + \bar{a}b \right) \left(|a|^2 + |b|^2 \right)
\end{aligned}$$

and

$$\begin{aligned}
(\mathbf{F} \times \mathbf{F}^*)_{\hat{\mathbf{j}}} &= 2ab \left(\bar{b}^2 - \bar{a}^2 \right) - 2\bar{a}\bar{b} \left(b^2 - a^2 \right) \\
&= 2 \left[a\bar{b}|b|^2 - \bar{a}b|a|^2 - \bar{a}b|b|^2 + a\bar{b}|a|^2 \right] \\
&= 2 \left[a\bar{b} \left(|a|^2 + |b|^2 \right) - \bar{a}b \left(|a|^2 + |b|^2 \right) \right] \\
&= 2 \left(a\bar{b} - \bar{a}b \right) \left(|a|^2 + |b|^2 \right)
\end{aligned}$$

and

$$(\mathbf{F} \times \mathbf{F}^*)_{\hat{\mathbf{k}}} = -\imath \left[\left(b^2 - a^2 \right) \left(\bar{a}^2 + \bar{b}^2 \right) + \left(\bar{b}^2 - \bar{a}^2 \right) \left(a^2 + b^2 \right) \right]$$

$$= -\imath \left[\bar{a}^2 b^2 - a^2 \bar{b}^2 - |a|^4 + |b|^4 + a^2 \bar{b}^2 - \bar{a}^2 b^2 - |a|^4 + |b|^4 \right]$$

$$= 2\imath \left[|a|^4 - |b|^4 \right] = 2\imath \left(|a|^2 + |b|^2 \right) \left(|a|^2 - |b|^2 \right)$$

and we find

$$\left(\frac{\mathbf{F} \times \mathbf{F}^*}{\mathbf{F} \cdot \mathbf{F}^*} \right) = \frac{2 \left(|a|^2 + |b|^2 \right)}{|d|^6} \frac{|d|^6}{2 \left(|a|^2 + |b|^2 \right)^2} \left(\imath (a\bar{b} + \bar{a}b), a\bar{b} - \bar{a}b, \imath \left(|a|^2 - |b|^2 \right) \right)$$

$$= \frac{1}{|a|^2 + |b|^2} \left(\imath (a\bar{b} + \bar{a}b), a\bar{b} - \bar{a}b, \imath \left(|a|^2 - |b|^2 \right) \right)$$

So, the normalized Poynting field for the Hopfion solution is

$$\hat{\mathbf{S}} = \frac{\mathbf{E} \times \mathbf{B}}{|\mathbf{E} \times \mathbf{B}|} = -\frac{1}{|a|^2 + |b|^2} \left(a\bar{b} + \bar{a}b, \imath (a\bar{b} - \bar{a}b), |a|^2 - |b|^2 \right) \tag{29}$$

Substituting the values of a and b, obtained from (24), we find that

$$\hat{\mathbf{S}} = \frac{1}{1 + x^2 + y^2 + (z - t)^2} \tag{30}$$

$$\left(2(x(z - t) - y), 2(x + y(z - t)), 1 + (z - t) - y^2 - x^2 \right)$$

An alternative derivation, due to Rañada [14,15], yields the following expressions for these fields, the advantage of doing this lies in the fact that they include the time dependence.

$$\mathbf{E} = \frac{1}{8\imath} \frac{\nabla \zeta \times \nabla \bar{\zeta}}{\left(1 + \bar{\zeta}\zeta \right)^2} \qquad \mathbf{B} = \frac{1}{8\imath} \frac{\nabla \eta \times \nabla \bar{\eta}}{\left(1 + \bar{\eta}\eta \right)^2} \tag{31}$$

$$\zeta(x, y, z, t) = \frac{(Ax + ty) + \imath(Az + t(A - 1))}{(tx - Ay) + \imath(A(A - 1) - tz)}$$

$$\eta(x, y, z, t) = \frac{(Az + t(A - 1)) + \imath(tx - Ay)}{(Ax + ty) + \imath(A(A - 1) - tz)}$$

with

$$A(x, y, z, t) = \frac{1}{2} \left(x^2 + y^2 + z^2 - t^2 + 1 \right)$$

This derivation utilizes the elegance of differential geometry and the tensor formalism of the electromagnetic field.

5.4   Verifications

To verify that this solution is indeed related to the Hopf map, we notice that if we normalize the electric and magnetic field expressions, then these vectors will all lie on the 2-sphere. After normalization we have that

$$\frac{\mathbf{E}}{|\mathbf{E}|} = \hat{\mathbf{E}} = \frac{1}{1 + x^2 + y^2 + z^2} \left(-1 - x^2 + y^2 + z^2, -2(xy - z), -2(y + xz) \right)$$

and

$$\frac{\mathbf{B}}{|\mathbf{B}|} = \hat{\mathbf{B}} = \frac{1}{1 + x^2 + y^2 + z^2} \left(2(xy + z), 1 - x^2 + y^2 - z^2, -2(x - yz) \right)$$

and we see that indeed $\hat{\mathbf{E}}$ and $\hat{\mathbf{B}}$ are results of a Hopf map. The explicit parameters of this map are

$$\hat{\mathbf{E}} = h \left(\frac{z}{\alpha}, \frac{-y}{\alpha}, \frac{x}{\alpha}, \frac{1}{\alpha} \right) \tag{32}$$

$$\tag{33}$$

$$\hat{\mathbf{B}} = h' \left(\frac{1}{\alpha}, \frac{y}{\alpha}, \frac{x}{\alpha}, \frac{z}{\alpha} \right) \tag{34}$$

where $h'(a, b, c, d) = (2(ad + bc), a^2 + b^2 - c^2 - d^2, 2(bd - ac))$ is a rotation through 90 de-

grees along an axis of the original Hopf map we defined above, and $\alpha^2 = 1 + x^2 + y^2 + z^2$. Similarly, for the Poynting field, we find that

$$\hat{\mathbf{S}} = h'' \left(\frac{1}{\beta}, \frac{z-t}{\beta}, \frac{y}{\beta}, \frac{x}{\beta} \right)$$

where $\beta^2 = 1 + x^2 + y^2 + (z-t)^2$ and h'' is, again, a rotation of the original Hopf map. This verifies that the solution is indeed a Hopfion solution.

5.5   Remarks

As the Poynting field, in this form (30), is valid for all time t, we see that the Hopf structure is preserved for the energy density that this beam of light carries. It should be noted that the electric and magnetic fields are dynamic. As time progresses, we find that the tori that the field lines define deform. This can be seen using the results from Rañada (31), with the actual time evolution shown in [6–8]. The Poynting field is the most interesting feature of this construction because this is the property that all solutions in the family share. This property for the family is referred to in the literature as the Robinson congruence [16], as mentioned earlier.

6   Generalized Solutions on Torus Knots

The Bateman method for generating solutions to Maxell's equations in vacuum, as we have seen, is extremely powerful and provides a nearly endless supply of interesting and compelling solutions. Using techniques from complex analysis and building upon the Hopfion solution described above, we can generate an entire family of solutions with the desirable property of topological invariance. In the Hopfion solution, all of the electric and magnetic field lines are linked circles, and they persist in that configuration for all time. However, this construction does not limit us to just consider linked circles. We are able to generate solutions that consist of linked torus knots.

6.1   Parameters

To generate these solutions we first recall a theorem from complex analysis [13]. For two complex numbers u and v such that $|u|^2 + |v|^2 = 1$ then $u^p \pm v^q = 0$ is the equation of a (p, q) torus knot, for p and q coprime integers. This is useful to us because we know that

$$S^3 = \left\{ (u, v) \in \mathbb{C}^2 \,\middle|\, |u|^2 + |v|^2 = 1 \right\}$$

With this theorem and the following choices for α and β for use in Bateman's construction

$$\alpha(x, y, z, t) = \frac{r^2 - t^2 - 1 + 2\imath z}{r^2 - (t - \imath)^2}, \qquad \beta(x, y, z, t) = \frac{2(x - \imath y)}{r^2 - (t - \imath)^2} \tag{35}$$

we can generate solutions with field lines that are (p, q) linked torus knots. Since we see that $|\alpha|^2 + |\beta|^2 = 1$ for all time t.

$$|\alpha|^2 = \frac{\left(r^2 - t^2 - 1\right)^2 + 4z^2}{\left(r^2 - t^2 + 1\right)^2 + 4t^2} \qquad \text{and} \qquad |\beta|^2 = \frac{4x^2 + 4y^2}{\left(r^2 - t^2 + 1\right)^2 + 4t^2}$$

and we get

$$|\alpha|^2 + |\beta|^2 = \frac{4r^2 + (r^2 - t^2 - 1)^2}{4t^2 + (r^2 - t^2 + 1)^2} = 1$$

Thus, this choice of α and β will indeed yield the desired torus knots. Furthermore, we have that

$$
\begin{aligned}
\nabla\alpha \cdot \nabla\alpha - \left(\frac{\partial\alpha}{\partial t}\right)^2 &= 0 \\
\nabla\beta \cdot \nabla\beta - \left(\frac{\partial\beta}{\partial t}\right)^2 &= 0 \\
\nabla\alpha \cdot \nabla\beta - \frac{\partial\alpha}{\partial t}\frac{\partial\beta}{\partial t} &= 0
\end{aligned}
\tag{36}
$$

and these expressions satisfy the requirements (6) to be valid functions for Bateman's construction. Making the obvious choice of $f(\alpha, \beta) = \alpha^p$ and $g(\alpha, \beta) = \beta^q$ we obtain:

$$
\begin{aligned}
\mathbf{F} = \nabla f(\alpha, \beta) \times \nabla g(\alpha, \beta) &= \nabla\alpha^p \times \nabla\beta^q \\
&= pq\alpha^{p-1}\beta^{q-1}\left(\nabla\alpha \times \nabla\beta\right)
\end{aligned}
\tag{37}
$$

where we now have that the Poynting field is given by this new $\nabla\alpha \times \nabla\beta$ term. With this formulation we find:

$$\nabla\alpha \times \nabla\beta = \frac{16}{d^3}\left(b^2 - a^2, -\imath\left(a^2 + b^2\right), 2ab\right)$$

where the definitions of a, b, and d are the same as for the Hopfion solution (24). Evidently, this is the exact expression that we had determined for the Poynting field in the Hopfion solution, up to a scaling factor. Therefore, we see that the Hopfion solution is really a specific case of this more generalized formulation with $p = q = 1$. Furthermore, the core electric and magnetic field lines now form linked torus knots, not simply circles, that fiber S^3. And these fibers form nested torus knots that fill all $\mathbb{R}^3$.

6.2   Remarks

We have determined that with this choice of α and β, we were able to construct a family of solutions that are related to the Hopfion solution. They all share the same Poynting field, but the structures of the corresponding electric and magnetic fields are much more complex. The topological structure of these fields is again preserved in time. The choice of $f = \alpha^p$ and $g = \beta^q$ allows us to obtain electric and magnetic field lines that form linked p, q torus knots that fill all space. This hearkens back to the Hopf fibration in that these field lines are again linked but now, instead of the fibers consisting of circles, they are instead torus knots.

The following section presents an algorithm to parameterize a Seifert surface for arbitrary torus knots.

7 Seifert Surfaces

The surface of the torus embedded in $\mathbb{R}^3$ is an important surface in the theory of knots. The study of knots is an ever-expanding field in pure mathematics and there are many seemingly simple questions that have gone unanswered. This section will discuss an interesting theorem, first proven in 1935, about knots as surface boundaries. It turns out that every knot can be the boundary of a closed and bounded orientable surface.

In 1934 the German mathematician Herbert Seifert developed a very clever algorithm [17] that produces a connected, compact and orientable surface such that the boundary of the surface is a given knot in Euclidean 3-space. The algorithm begins with an oriented knot (I will be using the trefoil knot as an example, but the algorithm works with any knot or link) projected onto any plane in 3-space. For simplicity I will use the xy-plane. The simplest parametrization of the trefoil knot is given by the equations:

$$
\begin{aligned}
x(t) &= r(t)\cos(pt) \\
y(t) &= r(t)\sin(pt) \\
z(t) &= \sin(qt)
\end{aligned}
\tag{38}
$$

where $r(t) = \cos(qt) + 2$. p and q are integers related to the topology of the knot. This parametrization places the trefoil knot on the surface of a torus embedded in 3-space. The torus can be thought of as two circles, one centered at the origin and the other tangent to the first circle oriented perpendicularly. This is represented by $T^2 = S^1 \times S^1$. So q is the number of times the knot circumnavigates the torus in the poloidal direction and p is the number of times the knot goes around in the toroidal direction. Using this parametrization, one can create any knot lying on the surface of the torus so long as p and q are coprime integers. For the trefoil knot $p = 2$ and $q = 3$.

The projection of the knot onto the xy-plane is easily done, simply let $z(t) = 0$. Using this projection, our knot will be an oriented curve in the plane with three crossings (see
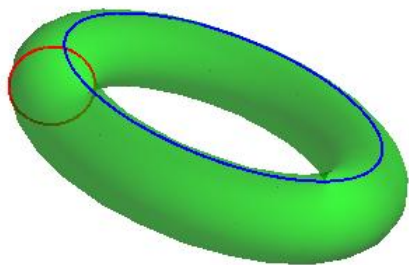
Figure 7: The torus T^2 with component circles shown. p is the number of times the knot goes around the blue circle. q is the number of times the knot goes around the red circle

(a)

(b)

(c)
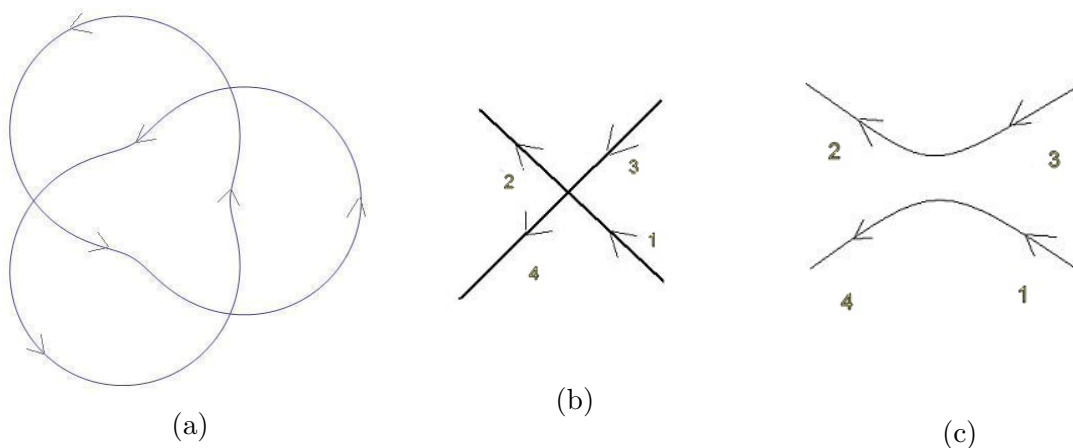
Figure 8: Deleting crossings. (a) Oriented trefoil knot projected onto xy-plane. (b) Close-up of one of the crossings. (c) After deleting the crossing.

Figure 8a). At each of these crossings there are two arrows coming in and two arrows going out. In Figure 8b it can be seen that $1 \to 2$ and $3 \to 4$. By reassigning these such that $1 \to 4$ and $3 \to 2$ we can delete the crossing as in Figure 8c.

7.1 'Top' and 'Bottom' Surfaces

Once the crossings have been deleted, we are left with two disconnected circles. Now we can move these circles so that they are in parallel planes and we can fill them in so that they are now discs (see Figure 9). This is easy enough to do theoretically, but in practice with an actual parametrized curve it is a bit more complicated. The crossing cannot in actuality be deleted, to do so would change the boundary of the surface being generated.

When parametrizing these 'top' and 'bottom' surfaces we must take care to associate their boundaries with the knot.
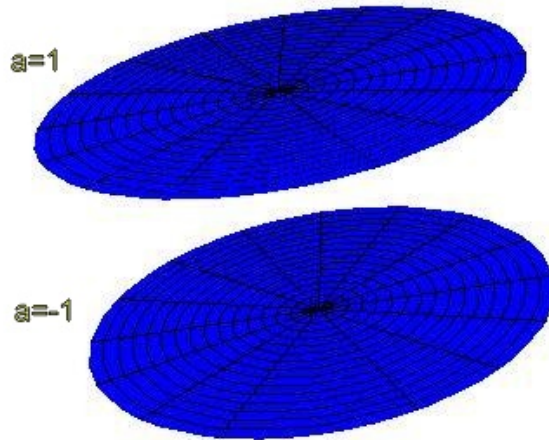
Figure 9: Two discs in parallel planes

To effectively delete the crossing, it is necessary to identify a point on the curve before and after the crossing. As each crossing is represented by two values of the parameter t this means that there will be four points identified at each crossing (see Figure 8c). Let C be the set of all times t that a crossing occurs. So

$$C = \{t_1, t_2, ..., t_n\} \text{ where } \frac{n}{2} \text{ is the number of crossings}$$

For the trefoil knot, t_1 and t_4 are one crossing, t_2 and t_5 are the next and t_3 and t_6 are the last one. To 'delete' the crossing it is necessary to choose a point just before and just after the t_i that the crossing occurs. So the various intervals of the parameter t that will be used for the 'top' surface boundary that lie on the knot are

$$(t_1 - \frac{1}{q}, t_1 + \frac{1}{pq}), (t_3 - \frac{1}{q}, t_3 + \frac{1}{pq}), \text{ and } (t_5 - \frac{1}{q}, t_5 + \frac{1}{pq})$$

34

Using intervals that depend on the values of p and q allows this process to be used for other knots, thus making this method not specific for the trefoil knot. The other three portions of the boundary for this surface will be straight lines connecting the ends of the portions of the boundary of the surface that lie on the knot (see Figure 10a). The parametrization for the first of these lines is given by:

$$X(T) = x(t_1 - \frac{1}{q}) * (1 - T) + x(t_3 + \frac{1}{pq}) * T$$
$$Y(T) = y(t_1 - \frac{1}{q}) * (1 - T) + y(t_3 + \frac{1}{pq}) * T \qquad (39)$$
$$Z(T) = z(t_1 - \frac{1}{q}) * (1 - T) + z(t_3 + \frac{1}{pq}) * T$$

where T is the parametrizing variable and the functions $x(t)$, $y(t)$, and $z(t)$ are the parametrization functions for the knot as in (38). Notice that

$$X(0) = x(t_1 - \frac{1}{q}) \text{ and } X(1) = x(t_3 + \frac{1}{pq})$$

which are the endpoints of the sections of the boundary that lie on the knot. The other

(a)   (b)
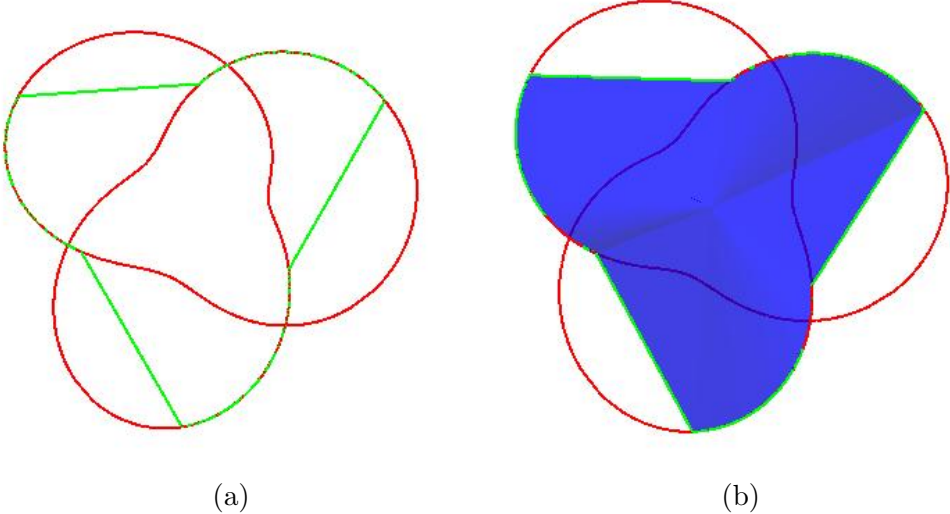
Figure 10: Generalization of the top and bottom surfaces. (a) The green curve is the boundary of our top surface; (b) The top surface with boundary

parametrizations are similar to this one, just change the endpoints. So, now that the boundaries are defined for these surfaces they can be parametrized.

To parametrize a disc in 3-space it is easiest to use polar coordinates. The equations are simply

$$X(r, \phi) = r \cos \phi$$

$$Y(r, \phi) = r \sin \phi$$

$$Z(r, \phi) = a$$

where r varies from 0 to the boundary of the disc, ϕ varies from 0 to 2π, and a is a
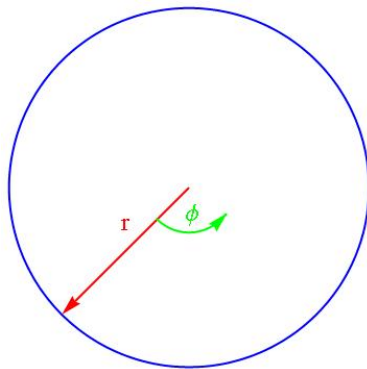
Figure 11: Parameterizing a disc. As r varies from 0 to the boundary and ϕ varies from 0 to 2π the circle is filled and becomes a disc

constant. Thus, any pair (r, ϕ) uniquely determines a point on the disc. Notice that the parametrization of the knot is a function of one variable, t, but the parametrization of a surface is a function of two variables, in this case r and ϕ. More commonly the variables u and v are used to parametrize a surface.

The 'top' and 'bottom' surfaces for our purposes will not be circular discs but they will be parametrized in an analogous way. In other words, they will be topologically equivalent to a circular disc. Since the boundaries of the surfaces being constructed are defined piecewise, it is necessary to define the surfaces piecewise. There will be six separate pieces for the trefoil knot. Alternating pieces will have their boundary on the knot and the other pieces will have their boundary be a straight line connecting the sections lying on the knot. Thus

the boundary of the 'top' and 'bottom' surfaces will be a closed curve (see Figure 10a).
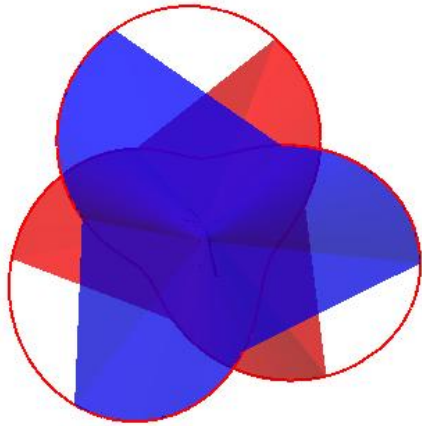
Figure 12: Actual top and bottom surfaces. The top surface is blue and the bottom surface is red

To parametrize a surface with this boundary, it is a simple matter of varying r from 0 to the boundary and varying ϕ from 0 to 2π. Since these surfaces must be at different 'heights' for the algorithm to work, choosing the center of the 'top' surface to be $(0, 0, a)$ and the center for the 'bottom' surface to be $(0, 0, -a)$ this condition is met (see Figure 12).

7.2 Twisted Bands

The final step in Seifert's algorithm is to reconnect the disjoint surfaces. To do this requires taking a band or strip, giving it a half twist, and identifying the ends of the band with the boundaries of the top and bottom surface. Giving the band a twist allows the surface to remain orientable while at the same time keeping the boundary of the surface on the knot. The reason this guarantees orientability is that both the top and bottom surfaces are oriented, they both have two distinct sides. The band that we are using also has two distinct sides and by giving the band a half twist and identifying boundaries, the top and bottom surfaces become connected and oriented with respect to each other. This is the crux of the algorithm and also the end of the algorithm. The surface we have constructed is closed, bounded, connected and oriented. Theoretically this is a fairly simple construction, but in working with a parameterized curve the difficulty is substantial.
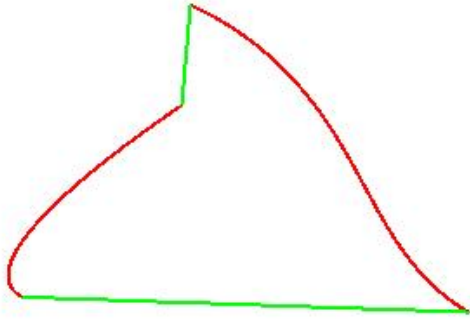
Figure 13: The boundary of the band. The green curves are part of the boundaries of the top and bottom surfaces. The red curves are sections of the trefoil knot.

The region that we are parametrizing is bounded by four curves. Two of these curves are sections of the trefoil knot, while the other two are straight lines given by the parametrization in (39). Recall that the straight lines are part of the boundaries of the top and bottom surfaces constructed in the previous section. Using u and v as the parameters for these surfaces and letting both parameters vary from 0 to 1, we arrive at the following parametrization:

$$X(u,v) = x(t_1 - \frac{1}{q} - \frac{\pi - 2}{q} v) * u + x(t_3 + \frac{1}{pq} + \frac{p\pi - 2}{pq} v) * (1 - u)$$

$$Y(u,v) = y(t_1 - \frac{1}{q} - \frac{\pi - 2}{q} v) * u + y(t_3 + \frac{1}{pq} + \frac{p\pi - 2}{pq} v) * (1 - u) \qquad (40)$$

$$Z(u,v) = z(t_1 - \frac{1}{q} - \frac{\pi - 2}{q} v) * u + z(t_3 + \frac{1}{pq} + \frac{p\pi - 2}{pq} v) * (1 - u)$$

This looks complicated at first glance, but upon closer inspection, the details become clear. When $u = 0$ or 1 and v is allowed to vary, this reduces to the parametrization of a section of the knot (i.e. the boundary of the band). When $v = 0$ or 1 and u is allowed to vary, the parametrization yields the boundaries shared by the top and bottom surfaces. Thus each pair (u, v) uniquely determines a point on the band.

The other bands have similar parametrizations, simply replacing t_1 with t_2 and t_3 with t_4, etc. Again, defining the intervals in terms of p and q make it possible to generalize this method for other knots. Since the boundary of the band coincides with the boundaries of

(a)

(b)
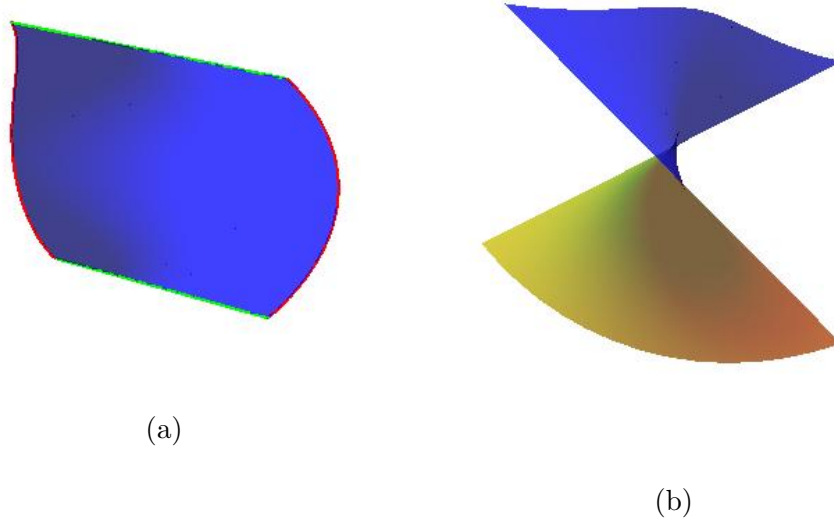
Figure 14: Twisted bands. (a) The band with its boundary; (b) A view of the band suggesting its twist.

the top and bottom surfaces, when the bands and surfaces are joined these are no longer boundaries but become a part of the resulting surface. The only boundary left to this surface is the knot itself and our surface is closed, bounded, connected and oriented thus completing the algorithm. It should be noted that this method of parametrizing a Seifert surface only works for $p = 2$ and q odd.
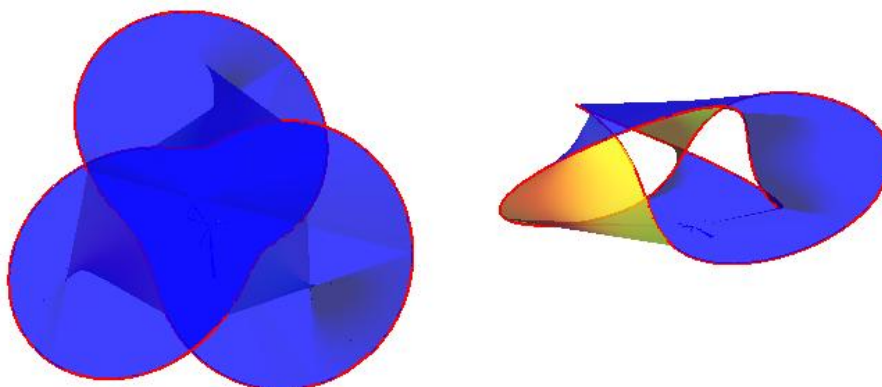
Figure 15: The finished Seifert surface for the trefoil knot

7.3   Verification of Stokes' Theorem

Theory

Stokes' Theorem states that the surface integral of the curl of a vector potential over a connected, compact, and orientable surface is equal to the line integral of the vector potential over the boundary of the surface. In 3-space this is represented symbolically by the equation

$$\iint_{\Sigma} (\nabla \times \mathbf{A}) \cdot d\mathbf{\Sigma} = \oint_{\partial \Sigma} \mathbf{A} \cdot d\mathbf{s} \tag{41}$$

where $\mathbf{A}$ is the vector potential, Σ is the surface, and $\partial\Sigma$ is the boundary of Σ (in this case the trefoil knot). The terms, $d\mathbf{s}$ and $d\mathbf{\Sigma}$, are the oriented line element of the boundary and the normal oriented surface element of the surface, respectively. The relationship of the vector potential $\mathbf{A}$ to the vector field $\mathbf{B}$ is given by

$$\mathbf{B} = \nabla \times \mathbf{A} \tag{42}$$

To define a vector field in Euclidean 3-space is a fairly straightforward process. Every point in space needs to have a vector assigned to it, relative to a fixed origin. The simplest vector field is the constant vector field in which every point in space will have the same vector assigned to it. In Cartesian coordinates,

$$\mathbf{B} = (0, 0, c)$$

where c is some constant. The vector potential that gives rise to this field is given by (again in Cartesian coordinates)

$$\mathbf{A} = (-\frac{c}{2} y, \frac{c}{2} x, 0) \tag{43}$$

Recall that the 'del' operator, ∇, is defined as

$$\nabla = \left(\frac{\partial}{\partial x}, \frac{\partial}{\partial y}, \frac{\partial}{\partial z} \right)$$

It is a simple calculation to verify (42) given this **A** and **B**.

The Right-Hand Side

Calculating $\mathrm{d}\mathbf{s}$ for the trefoil knot is fairly simple and the evaluation of the RHS of Stokes'
Theorem (41) can be performed analytically. As $\mathbf{s}(t)$ is the parametrization of the trefoil
knot given by (38) the calculation of $\mathrm{d}\mathbf{s}$ is carried out as follows:

$$\mathbf{s}(t) = (x(t),\, y(t),\, z(t))$$

$$\frac{\mathrm{d}\mathbf{s}}{\mathrm{d}t} = \left(\frac{\mathrm{d}x}{\mathrm{d}t},\, \frac{\mathrm{d}y}{\mathrm{d}t},\, \frac{\mathrm{d}z}{\mathrm{d}t} \right)$$

$$\mathrm{d}\mathbf{s} = \left(\frac{\mathrm{d}x}{\mathrm{d}t},\, \frac{\mathrm{d}y}{\mathrm{d}t},\, \frac{\mathrm{d}z}{\mathrm{d}t} \right) \mathrm{d}t \tag{44}$$

From this calculation it is possible to evaluate the RHS of Stokes' Theorem. By substituting
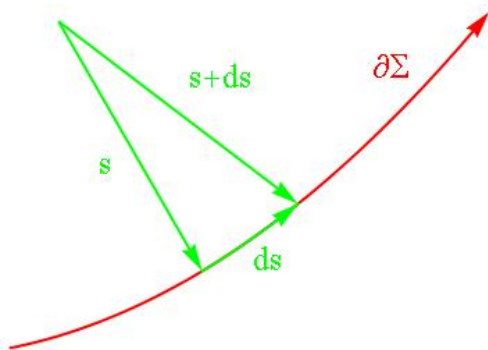
Figure 16: Line elements for the contour integral. The line element $\mathrm{d}\mathbf{s}$ is the change in $\mathbf{s}$ that results from a small change in the parameter t

(43) and (44) into the RHS of (41) and evaluating

$$\oint_{\partial\Sigma} \mathbf{A} \cdot \mathrm{d}\mathbf{s} = \int_0^{2\pi} \left[-\frac{c}{2} \frac{\mathrm{d}x}{\mathrm{d}t} y(t) + \frac{c}{2} \frac{\mathrm{d}y}{\mathrm{d}t} x(t) \right] \mathrm{d}t = 9c\pi$$

The Left-Hand Side

As mentioned before, the RHS is the easy part of verifying Stokes' Theorem. The real difficulty arises in the calculation of the surface area elements. For a surface to be orientable it must have a 'direction' assigned to it. This direction is best thought of as a unit 'normal' vector (a vector that is directed perpendicular to the surface). Every point (u, v) of the surface has a normal vector, $\hat{\mathbf{n}}$, associated with it and by definition $\|\hat{\mathbf{n}}\| = 1$.

(a)   (b)
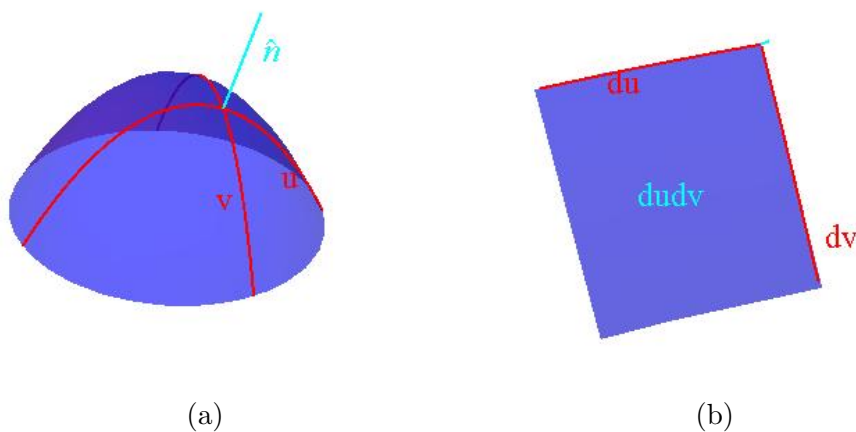
Figure 17: Vectors normal to a surface. (a) The normal vector $\hat{\mathbf{n}}$ is perpendicular to the surface; (b) The oriented surface area element $d\mathbf{\Sigma}$ has the direction of $\hat{\mathbf{n}}$ and its magnitude is given by the area of the surface element $dudv$

The surface area element is calculated by taking the cross product of the line elements $d\mathbf{u}$ and $d\mathbf{v}$. These are defined in an analogous way as $d\mathbf{s}$ was defined in (44). The only difference is that $d\mathbf{u}$ and $d\mathbf{v}$ are functions of u and v. Using a parametrization of the surface like that given in Section 7.2

$$d\mathbf{u} = \left(\frac{\partial X}{\partial u}, \frac{\partial Y}{\partial u}, \frac{\partial Z}{\partial u} \right) du \quad \text{and} \quad d\mathbf{v} = \left(\frac{\partial X}{\partial v}, \frac{\partial Y}{\partial v}, \frac{\partial Z}{\partial v} \right) dv \tag{45}$$

From these definitions, it is clear that

$$\hat{\mathbf{n}} = \frac{d\mathbf{u} \times d\mathbf{v}}{\|d\mathbf{u} \times d\mathbf{v}\|}$$

and since $d\mathbf{u} \perp d\mathbf{v}$ then $\|d\mathbf{u} \times d\mathbf{v}\| = dudv$ and $d\mathbf{\Sigma} = \hat{\mathbf{n}}\,dudv$. This result becomes

$$d\mathbf{\Sigma} = \hat{\mathbf{n}}\,dudv = \frac{d\mathbf{u} \times d\mathbf{v}}{\|d\mathbf{u} \times d\mathbf{v}\|}\|d\mathbf{u} \times d\mathbf{v}\| = d\mathbf{u} \times d\mathbf{v} \tag{46}$$

This form of $d\mathbf{\Sigma}$ will be useful in the calculations needed to evaluate the LHS of (41). Since the Seifert surface is defined in multiple sections (there are 15 separate sections for the trefoil knot surface), it is necessary to evaluate the surface area elements, $d\mathbf{\Sigma}$, for each of these sections separately. However, the method used is the same for each section. Substituting (42) and (46) into (41) yields

$$\iint_{\Sigma} (\nabla \times \mathbf{A}) \cdot d\mathbf{\Sigma} = \iint_{\Sigma} \mathbf{B} \cdot (d\mathbf{u} \times d\mathbf{v}) \tag{47}$$

Evaluating $d\mathbf{u} \times d\mathbf{v}$ using (44) and switching to the more compact notation $\partial X/\partial u = X_u$, and so on.

$$d\mathbf{u} \times d\mathbf{v} = (Y_u Z_v - Y_v Z_u, X_v Z_u - X_u Z_v, X_u Y_v - X_v Y_u)\,dudv$$

and since $\mathbf{B} = (0, 0, c)$ this complicated term simplifies to

$$\iint_{\Sigma} \mathbf{B} \cdot (d\mathbf{u} \times d\mathbf{v}) = \int_0^1 \int_0^1 c\,(X_u Y_v - X_v Y_u)\,dudv$$

Due to the complicated nature of the parametrizations involved, this integral cannot be solved analytically for every section of the Seifert surface. Using the `NIntegrate` function in *Mathematica* with $c = 1$ with a working precision of 20 digits yields

$$\iint_{\Sigma} (\nabla \times \mathbf{A}) \cdot d\mathbf{\Sigma} = 28.274333882308108973$$

Comparing this value with the value obtained for the RHS of 9π shows that the error between the two methods is on the order of 10^{-14}. The two sides of Stokes' Theorem are in excellent agreement for this Seifert surface.
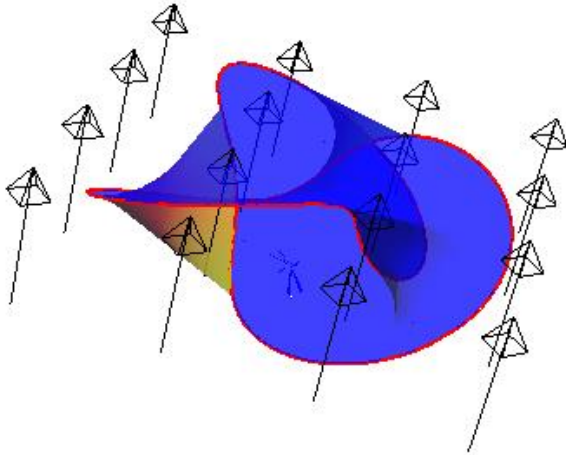
Figure 18: Full surface with field. The Seifert surface embedded within the constant vector field $\mathbf{B} = (0, 0, c)$.

8 Conclusions

As we have observed, the Hopfion solution is a fairly peculiar phenomenon, to say nothing of the generalized solutions on more complicated torus knot structures. These light fields are indeed allowed by Maxwell's theory, as they are solutions to the relevant equations. The Poynting fields of both the Hopfion solution and the generalised torus knot solutions possess a common structure that is preserved in time, allowing for the encoding of information in the energy flow of these beams of light. When these beams are able to be produced in a laboratory they may yield answers to the problems of decoherence that have hindered the development of an adequate quantum computer to date. The construction of a topological quantum computer would rely heavily on such phenomena, in light and matter both. The applications of these types of light fields, once produced, will be far reaching. The reason for this is the ability to encode information in light, not only through frequency and amplitude modulation, but also in this energy modulation. This encoding, being of a topological nature, is very robust.

Other areas where knots and topology have received recent attention are quantum field theory [19], statistical mechanics, biology [1] (in the areas of protein folding and the structure of DNA), and fluid dynamics, to name but a few. This relatively new area of study is ripe with new solutions to interesting and challenging questions.

An additional area of interest and further research would lie on the experimental side. Creating these types of beams of light in the laboratory would be the logical next step in furthering their study. When the Hopfion solution is expanded as a linear combination of vector spherical harmonics it is found that they it possesses a surprisingly simple expansion, consisting of only two terms; a single transverse electric term and a single transverse magnetic term. This suggests the use of tightly focused Laguerre-Gaussian beams in the production of such light in the laboratory [7].

Appendix A   Parameterizing a Seifert Surface of the

Trefoil Knot

I have here included the *Mathematica* notebook I wrote to parameterize the Seifert Surface outlined in this paper.

$p = 2; q = 3; a = 1;$

r1[t_] = Cos[q * t] + 2;

x1[t_] = r1[t] * Cos[p * t];

y1[t_] = r1[t] * Sin[p * t];

z1[t_] = a * Sin[q * t];

   These are the times at which the knot crosses itself when viewed from above (i.e. z = 0), for p and q coprime

time1 = Range[Pi/(p * q), Pi, p * Pi/(p * q)];

time2 = time1 + Pi;

time3 = time2 + Pi;

x1[time1] == x1[time2]

y1[time1] == y1[time2]

True

True

time = Flatten[{{time1}, {time2}, {time3}}]

$\left\{ \frac{\pi}{6}, \frac{\pi}{2}, \frac{5\pi}{6}, \frac{7\pi}{6}, \frac{3\pi}{2}, \frac{11\pi}{6}, \frac{13\pi}{6}, \frac{5\pi}{2}, \frac{17\pi}{6} \right\}$

Table[{x1[t, δ], y1[t, δ], z1[t, δ]}, {δ, 0, 2π, π/4}];

c = ParametricPlot3D[{x1[t], y1[t], z1[t]}, {t, 0, 2 * Pi}, PlotStyle → {Red},

Axes → False, Boxed → False]

Clear[f, g, h];

f = Range[Length[time1]];

$g = \text{Range}[\text{Length}[\text{time1}]];$

$h = \text{Range}[\text{Length}[\text{time1}]];$

(*getting the different boundaries for the siefert algorithm*)

$\text{Do}[f[[i]] = \text{ParametricPlot3D}[\{\text{x1}[t], \text{y1}[t], \text{z1}[t]\},$

$\{t, \text{time}[[2i-1]] - 1/q, \text{time}[[2i-1]] + 1/(p*q)\},$

$\text{PlotStyle} \rightarrow \{\text{Green}, \text{Thick}\}], \{i, 1, \text{Length}[\text{time1}]\}];$

$\text{Do}[$

$h[[i]] = \text{ParametricPlot3D}[$

$\{\text{x1}[\text{time}[[2i-1]] - 1/q] * (1-t) + \text{x1}[\text{time}[[2i+(q-p)]] + 1/(p*q)] * t,$

$\text{y1}[\text{time}[[2i-1]] - 1/q] * (1-t) + \text{y1}[\text{time}[[2i+(q-p)]] + 1/(p*q)] * t,$

$\text{z1}[\text{time}[[2i-1]] - 1/q] * (1-t) + \text{z1}[\text{time}[[2i+(q-p)]] + 1/(p*q)] * t\},$

$\{t, 0, 1\}, \text{PlotStyle} \rightarrow \{\text{Green}, \text{Thick}\}], \{i, 1, \text{Length}[\text{time1}]\}];$

$\text{Do}[$

$g[[i]] = \text{ParametricPlot3D}[$

$\{\text{x1}[\text{time}[[2i]]] + 1/q] * (1-t) + \text{x1}[\text{time}[[2i-(q-p)]]] * 1/(p*q)] * t,$

$\text{y1}[\text{time}[[2i]]] + 1/q] * (1-t) + \text{y1}[\text{time}[[2i-(q-p)]]] + 1/(p*q)] * t,$

$\text{z1}[\text{time}[[2i]]] + 1/q] * (1-t) + \text{z1}[\text{time}[[2i-(q-p)]]] + 1/(p*q)] * t\},$

$\{t, 0, 1\}, \text{PlotStyle} \rightarrow \{\text{Blue}, \text{Thick}\}], \{i, 1, \text{Length}[\text{time1}]\}];$

$\text{Show}[\{c, f, h\}, \text{PlotRange} \rightarrow \text{All}, \text{Axes} \rightarrow \text{False}, \text{Boxed} \rightarrow \text{False},$

$\text{ViewVector} \rightarrow \{\{0, 0, 10\}, \{0, 0, 0\}\}]$

    Parameterizing the top and bottom surface

$\text{topx}[\text{u}\_, \text{v}\_] = \text{x1}[u] * v;$

$\text{topy}[\text{u}\_, \text{v}\_] = \text{y1}[u] * v;$

$\text{topz}[\text{u}\_, \text{v}\_] = a * (1-v) + \text{z1}[u] * v;$

$\text{bottomx}[\text{u}\_, \text{v}\_] = \text{x1}[u] * v;$

$\text{bottomy}[\text{u}\_, \text{v}\_] = \text{y1}[u] * v;$

$\text{bottomz}[\text{u}\_, \text{v}\_] = -a * (1-v) + \text{z1}[u] * v;$

top = Range[time1];

topa = Range[time1];

bottom = Range[time1];

bottoma = Range[time1];

Do[top[[i]] = ParametricPlot3D[{topx[u, v], topy[u, v], topz[u, v]},

$\{u, \text{time}[[2i - 1]] - 1/q, \text{time}[[2i - 1]] + 1/(p * q)\}, \{v, 0, 1\},$

PlotStyle → {Opacity[.75], FaceForm[Yellow, Blue]}, Mesh → None],

$\{i, 1, \text{Length}[\text{time1}]\}];$

Do[

topa[[i]] =

ParametricPlot3D[

$\{(x1[\text{time}[[2i - 1]] - 1/q] * u + x1[\text{time}[[2i + (q - p)]] + 1/(p * q)] * (1 - u)) * v,$

$(y1[\text{time}[[2i - 1]] - 1/q] * u + y1[\text{time}[[2i + (q - p)]] + 1/(p * q)] * (1 - u)) * v,$

$(z1[\text{time}[[2i - 1]] - 1/q] * u + z1[\text{time}[[2i + (q - p)]] + 1/(p * q)] * (1 - u)) * v +$

$a * (1 - v)\}, \{u, 0, 1\}, \{v, 0, 1\},$

PlotStyle → {Opacity[.75], FaceForm[Yellow, Blue]}, Mesh → None],

$\{i, 1, \text{Length}[\text{time1}]\}]$

Do[

bottom[[i]] = ParametricPlot3D[{bottomx[u, v], bottomy[u, v], bottomz[u, v]},

$\{u, \text{time}[[2i]] + 1/q, \text{time}[[2i]] - 1/(p * q)\}, \{v, 0, 1\},$

PlotStyle → {Opacity[.75], FaceForm[Yellow, Blue]}, Mesh → None],

$\{i, 1, \text{Length}[\text{time1}]\}];$

Do[

bottoma[[i]] =

ParametricPlot3D[

$\{(x1[\text{time}[[2i + q - 1]] + 1/q] * (1 - u) + x1[\text{time}[[2i]] - 1/(p * q)] * u) * v,$

$(y1[\text{time}[[2i + q - 1]] + 1/q] * (1 - u) + y1[\text{time}[[2i]] - 1/(p * q)] * u) * v,$

$(z1[\text{time}[[2i + q - 1]]] + 1/q) * (1 - u) + z1[\text{time}[[2i]]] - 1/(p * q)] * u) * v -$

$a * (1 - v)\}, \{u, 0, 1\}, \{v, 0, 1\},$

$\text{PlotStyle} \to \{\text{Opacity}[.75], \text{FaceForm}[\text{Yellow}, \text{Blue}]\}, \text{Mesh} \to \text{None}],$

$\{i, 1, \text{Length}[\text{time1}]\}]$

$\text{Show}[\{c, f, h, \text{top}, \text{topa}\}, \text{PlotRange} \to \text{All}, \text{ViewVector} \to \{\{0, 0, 10\}, \{0, 0, 0\}\},$

$\text{Axes} \to \text{False}, \text{Boxed} \to \text{False}]$

$\text{band} = \text{Range}[\text{Length}[\text{time1}]];$

$\text{Do}[$

$\text{band}[[i]] = \text{ParametricPlot3D}[$

$\{x1[\text{time}[[2i - 1]]] - 1/q - v * (p * \text{Pi} - 2p)/(p * q)] * u +$

$x1[\text{time}[[2i + (q - p)]]] + 1/(p * q) + v * (p * \text{Pi} - 2)/(p * q)] * (1 - u),$

$y1[\text{time}[[2i - 1]]] - 1/q - v * (p * \text{Pi} - 2p)/(q * p)] * u +$

$y1[\text{time}[[2i + (q - p)]]] + 1/(p * q) + v * (p * \text{Pi} - 2)/(p * q)] * (1 - u),$

$z1[\text{time}[[2i - 1]]] - 1/q - v * (p * \text{Pi} - 2p)/(q * p)] * u +$

$z1[\text{time}[[2i + (q - p)]]] + 1/(p * q) + v * (p * \text{Pi} - 2)/(p * q)] * (1 - u)\},$

$\{u, 0, 1\}, \{v, 0, 1\}, \text{PlotStyle} \to \{\text{Opacity}[.75], \text{FaceForm}[\text{Yellow}, \text{Blue}]\},$

$\text{Mesh} \to \text{None}], \{i, 1, \text{Length}[\text{time1}]\}];$

$\text{surface} = \{\text{top}, \text{bottom}, \text{topa}, \text{bottoma}, \text{band}\};$

$\text{Show}[\{c, \text{surface}\}, \text{PlotRange} \to \text{All}, \text{ViewVector} \to \{\{0, 0, 10\}, \{0, 0, 0\}\},$

$\text{Boxed} \to \text{False}, \text{Axes} \to \text{False}]$

Appendix B   Verification of Stokes' Theorem

This section contains the notebook I created to verify Stokes' theorem for the Seifert surface generated in the previous appendix.

Verification of Stokes' Theorem requires a vector field. We'll start with the simplest case, a constant field

Clear[x, y, z, r, α]

subs = {$r \to$ Sqrt[x^2 + y^2 + z^2], $\alpha \to$ Sqrt[x^2 + y^2]};

vectpotential[x_, y_, z_] = FullSimplify[{$-y, x, 0$}/.subs];

bfield[x_, y_, z_] = FullSimplify[Curl[vectpotential[x, y, z], {x, y, z}]];

vf = VectorPlot3D[bfield[x, y, z], {$x, -3, 3$}, {$y, -3, 3$}, {$z, -1.5, 1.5$}, VectorPoints $\to$ {3, 3, 2},

VectorStyle $\to$ Blue, VectorScale $\to$ .3];

Show[{surface, vf}, PlotRange $\to$ All, Boxed $\to$ False, Axes $\to$ False]

I will proceed to verify Stokes' Theorem, which states that the flux of the curl of the vector field through the surface is equal to the line integral over the boundary.

LHS= $\int \left(\vec{\nabla} \times \vec{X} \right) \cdot \vec{n} \, d\Omega$

RHS= $\int \vec{X} \cdot d\vec{s}$

The curl of the vector potential is our B field. The flux of the curl of the vector potential is simply the flux of our B field through the surface.

Since the surface is defined in pieces, we must integrate it in pieces, this will be a lengthy process. We'll do the line integral first, it's much simpler and it will verify our result.

ds = {D[x1[t], t], D[y1[t], t], D[z1[t], t]}

{$-2(2 + \text{Cos}[3t])\text{Sin}[2t] - 3\text{Cos}[2t]\text{Sin}[3t], 2\text{Cos}[2t](2 + \text{Cos}[3t]) - 3\text{Sin}[2t]\text{Sin}[3t], 3\text{Cos}[3t]$}

vectpotential[x1[t], y1[t], z1[t]].ds;

rhs = Integrate[vectpotential[x1[t], y1[t], z1[t]].ds, {$t, 0, 2$Pi}]

18π

rhs = NIntegrate[vectpotential[x1[t], y1[t], z1[t]].ds, {$t, 0, 2\pi$}, WorkingPrecision $\to$ 20]

56.548667764616278293

$N[18\pi, 20]$

56.548667764616278292

Now look at getting the normal vectors for the surface...

center = $\{0, 0, 0\}$;

fluxtop = Range[time1];

fluxbottom = Range[time1];

fluxtopa = Range[time1];

fluxbottoma = Range[time1];

fluxband = Range[time1];

normtopa = Range[time1];

normbottoma = Range[time1];

normband = Range[time1];

normtop = Cross[$\{D[\text{topx}[u, v], u], D[\text{topy}[u, v], u], D[\text{topz}[u, v], u]\}$,

$\{D[\text{topx}[u, v], v], D[\text{topy}[u, v], v], D[\text{topz}[u, v], v]\}$];

normbottom = Cross[$\{D[\text{bottomx}[u, v], u], D[\text{bottomy}[u, v], u], D[\text{bottomz}[u, v], u]\}$,

$\{D[\text{bottomx}[u, v], v], D[\text{bottomy}[u, v], v], D[\text{bottomz}[u, v], v]\}$];

Do[

normtopa$[[i]]$ =

Cross[$\{D[\text{center}[[1]] * (1 - v) + (\text{x1}[\text{time}[[2i - 1]]] - 1/q] * u + \text{x1}[\text{time}[[2i + (q - p)]]]$

$+ 1/(p * q)] * (1 - u)) * v, u]$,

$D[\text{center}[[2]] * (1 - v) + (\text{y1}[\text{time}[[2i - 1]]] - 1/q] * u + \text{y1}[\text{time}[[2i + (q - p)]]]$

$+ 1/(p * q)] * (1 - u)) * v, u]$,

$D[(\text{z1}[\text{time}[[2i - 1]]] - 1/q] * u + \text{z1}[\text{time}[[2i + (q - p)]]] + 1/(p * q)] * (1 - u)) * v$

$+ (\text{center}[[3]] + a) * (1 - v), u]\}$,

$\{D[\text{center}[[1]] + (1 - v) + (\text{x1}[\text{time}[[2i - 1]]] - 1/q] * u + \text{x1}[\text{time}[[2i + (q - p)]]]$

$+ 1/(p * q)] * (1 - u)) * v, v]$,

51

$D[\text{center}[[2]] + (1 - v) + (\text{y1}[\text{time}[[2i - 1]]] - 1/q * u + \text{y1}[\text{time}[[2i + (q - p)]]]$

$+1/(p * q)] * (1 - u)) * v, v],$

$D[(\text{z1}[\text{time}[[2i - 1]]] - 1/q * u + \text{z1}[\text{time}[[2i + (q - p)]]] + 1/(p * q)] * (1 - u)) * v$

$+(\text{center}[[3]] + a) * (1 - v), v]\}],$

$\{i, 1, \text{Length}[\text{time1}]\}]$

Do[

normbottoma$[[i]] =$

$\text{Cross}[\{D[\text{center}[[1]] * (1 - v) + (\text{x1}[\text{time}[[2i + q - 1]]] + 1/q] * (1 - u)$

$+\text{x1}[\text{time}[[2i]]] - 1/(p * q)] * u) * v, u],$

$D[\text{center}[[2]] * (1 - v) + (\text{y1}[\text{time}[[2i + q - 1]]] + 1/q] * (1 - u)$

$+\text{y1}[\text{time}[[2i]]] - 1/(p * q)] * u) * v, u],$

$D[(\text{z1}[\text{time}[[2i + q - 1]]] + 1/q] * (1 - u) + \text{z1}[\text{time}[[2i]]] - 1/(p * q)] * u) * v$

$+(\text{center}[[3]] + -a) * (1 - v), u]\},$

$\{D[\text{center}[[1]] * (1 - v) + (\text{x1}[\text{time}[[2i + q - 1]]] + 1/q] * (1 - u)$

$+\text{x1}[\text{time}[[2i]]] - 1/(p * q)] * u) * v, v],$

$D[\text{center}[[2]] * (1 - v) + (\text{y1}[\text{time}[[2i + q - 1]]] + 1/q] * (1 - u)$

$+\text{y1}[\text{time}[[2i]]] - 1/(p * q)] * u) * v, v],$

$D[(\text{z1}[\text{time}[[2i + q - 1]]] + 1/q] * (1 - u) + \text{z1}[\text{time}[[2i]]] - 1/(p * q)] * u) * v$

$+(\text{center}[[3]] + -a) * (1 - v), v]\}],$

$\{i, 1, \text{Length}[\text{time1}]\}]$

Do[

normband$[[i]] =$

Cross[

$\{D[\text{x1}[\text{time}[[2i - 1]]] - 1/q - v * (p * \text{Pi} - 2p)/(p * q)] * u+$

$\text{x1}[\text{time}[[2i + (q - p)]]] + 1/(p * q) + v * (p * \text{Pi} - 2)/(p * q)] * (1 - u), u],$

$D[\text{y1}[\text{time}[[2i - 1]]] - 1/q - v * (p * \text{Pi} - 2p)/(q * p)] * u+$

$\text{y1}[\text{time}[[2i + (q - p)]]] + 1/(p * q) + v * (p * \text{Pi} - 2)/(p * q)] * (1 - u), u],$

$D[\mathrm{z1}[\mathrm{time}[[2i-1]]-1/q-v*(p*\mathrm{Pi}-2p)/(q*p)]*u+$

$\mathrm{z1}[\mathrm{time}[[2i+(q-p)]]+1/(p*q)+v*(p*\mathrm{Pi}-2)/(p*q)]*(1-u),u]\},$

$\{D[\mathrm{x1}[\mathrm{time}[[2i-1]]-1/q-v*(p*\mathrm{Pi}-2p)/(p*q)]*u+$

$\mathrm{x1}[\mathrm{time}[[2i+(q-p)]]+1/(p*q)+v*(p*\mathrm{Pi}-2)/(p*q)]*(1-u),v],$

$D[\mathrm{y1}[\mathrm{time}[[2i-1]]-1/q-v*(p*\mathrm{Pi}-2p)/(q*p)]*u+$

$\mathrm{y1}[\mathrm{time}[[2i+(q-p)]]+1/(p*q)+v*(p*\mathrm{Pi}-2)/(p*q)]*(1-u),v],$

$D[\mathrm{z1}[\mathrm{time}[[2i-1]]-1/q-v*(p*\mathrm{Pi}-2p)/(q*p)]*u+$

$\mathrm{z1}[\mathrm{time}[[2i+(q-p)]]+1/(p*q)+v*(p*\mathrm{Pi}-2)/(p*q)]*(1-u),v]\}],\{i,1,\mathrm{Length}[\mathrm{time1}]\}]$

Now that we have the normal vectors to the surface we can calculate the flux of the curl throught the surface.

Do[fluxtop[[i]] = NIntegrate[bfield[topx[u, v], topy[u, v], topz[u, v]].normtop,

$\{u, \mathrm{time}[[2i-1]]-1/q, \mathrm{time}[[2i-1]]+1/(p*q)\}, \{v, 1, 0\}, \mathrm{WorkingPrecision} \to 10]$,

$\{i, 1, \mathrm{Length}[\mathrm{time1}]\}]$

fluxtop

$\{5.107618972, 5.107618972, 5.107618972\}$

Do[fluxbottom[[i]] = NIntegrate[bfield[bottomx[u, v], bottomy[u, v], bottomz[u, v]].normbottom,

$\{u, \mathrm{time}[[2i]]+1/q, \mathrm{time}[[2i]]-1/(p*q)\}, \{v, 0, 1\}, \mathrm{WorkingPrecision} \to 20], \{i, 1, \mathrm{Length}[\mathrm{time1}]\}]$

fluxbottom

$\{5.1076192807870119981, 5.1076192807870119981, 5.1076192807870119981\}$

Do[

fluxtopa[[i]] =

NIntegrate[

bfield[center[[1]] $* (1-v) + (\mathrm{x1}[\mathrm{time}[[2i-1]]] - 1/q] * u + \mathrm{x1}[\mathrm{time}[[2i+(q-p)]]]$

$+1/(p*q)] * (1-u)) * v,$

center[[2]] $* (1-v) + (\mathrm{y1}[\mathrm{time}[[2i-1]]] - 1/q] * u$

$+\mathrm{y1}[\mathrm{time}[[2i+(q-p)]]] + 1/(p*q)] * (1-u)) * v,$

$(\mathrm{z1}[\mathrm{time}[[2i-1]]] - 1/q] * u+$

z1[time[[2i + (q − p)]] + 1/(p * q)] * (1 − u)) * v + (center[[3]] + a) * (1 − v)].

normtopa[[i]], {u, 0, 1}, {v, 1, 0}, WorkingPrecision → 20], {i, 1, Length[time1]}]

fluxtopa

{3.2775020027879794514, 7.1862221674959157785, 1.0549744068390007669}

Do[

fluxbottoma[[i]] =

NIntegrate[bfield[center[[1]] * (1 − v) + (x1[time[[2i + q − 1]] + 1/q] * (1 − u)

+x1[time[[2i]] − 1/(p * q)] * u) * v,

center[[2]] * (1 − v) + (y1[time[[2i + q − 1]] + 1/q] * (1 − u) + y1[time[[2i]] − 1/(p * q)] * u) * v,

(z1[time[[2i + q − 1]] + 1/q] * (1 − u)

+z1[time[[2i]] − 1/(p * q)] * u) * v + (center[[3]] + −a) * (1 − v)].

normbottoma[[i]], {u, 1, 0}, {v, 0, 1}, WorkingPrecision → 20], {i, 1, Length[time1]}]

fluxbottoma

{3.8395661923742986656, 3.8395661923742986656, 3.8395661923742986656}

Do[

fluxband[[i]] =

NIntegrate[

bfield[x1[time[[2i − 1]] − 1/q − v * (p * Pi − 2p)/(p * q)] * u+

x1[time[[2i + (q − p)]] + 1/(p * q) + v * (p * Pi − 2)/(p * q)] * (1 − u),

y1[time[[2i − 1]] − 1/q − v * (p * Pi − 2p)/(q * p)] * u+

y1[time[[2i + (q − p)]] + 1/(p * q) + v * (p * Pi − 2)/(p * q)] * (1 − u),

z1[time[[2i − 1]] − 1/q − v * (p * Pi − 2p)/(q * p)] * u+

z1[time[[2i + (q − p)]] + 1/(p * q) + v * (p * Pi − 2)/(p * q)] * (1 − u)].normband[[i]], {u, 0, 1},

{v, 1, 0}, WorkingPrecision → 20], {i, 1, Length[time1]}]

fluxband

{0.95518497521611798771, 0.95518497521611798771, 0.95518497521611798771}

unit = ConstantArray[1, Length[time1]]

$\{1, 1, 1\}$

lhs $= N[\text{fluxtop.unit} + \text{fluxbottom.unit} + \text{fluxtopa.unit} + \text{fluxbottoma.unit} + \text{fluxband.unit}, 20]$

56.54866684

$N[\text{Abs}[\text{lhs} - \text{rhs}], 16]$

9.263068722323072703448477168302 62.781415139614438*^-7

Appendix C   Visualizations of the Hopf Fibration

These are the routines I wrote to generate the figures in the body of my thesis.

(*Clearing variables*)

Clear[a, b, c, d]

(*StereographicProjection$S^3 \to R^3$*)

$s[$a_, b_, c_, d_$] = \{a/(1-d), b/(1-d), c/(1-d)\}$;

(*LinkednatureoffibersfortworandomlygeneratedpointsonS^2*)

subs1 = $\{\phi$->RandomReal[$\{0, 2\pi\}$]$, \theta \to$ RandomReal[$\{0, \pi\}$]$\}$;

subs2 = $\{\phi$->RandomReal[$\{0, 2\pi\}$]$, \theta \to$ RandomReal[$\{0, \pi\}$]$\}$;

points = Graphics3D[$\{$Opacity[.3], Yellow, Sphere[$\{0, 0, 0\}$], PointSize[Large],

Opacity[1], Red, Point[$\{$Sin[θ]Cos[ϕ], Sin[θ]Sin[ϕ], Cos[θ]$\}$/.subs1], Blue,

Point[$\{$Sin[θ]Cos[ϕ], Sin[θ]Sin[ϕ], Cos[θ]$\}$/.subs2]$\}$, Axes $\to$ False,

Boxed $\to$ False, AxesOrigin $\to \{0, 0, 0\}$, Ticks $\to$ None];

circles =

ParametricPlot3D[

$\{s[$Cos[$\phi/2 + \xi$]Cos[$\theta/2$], Sin[$\phi/2 + \xi$]Cos[$\theta/2$], Cos[$\xi - \phi/2$]Sin[$\theta/2$],

Sin[$\xi - \phi/2$]Sin[$\theta/2$]]/.subs1,

$s[$Cos[$\phi/2 + \xi$]Cos[$\theta/2$], Sin[$\phi/2 + \xi$]Cos[$\theta/2$], Cos[$\xi - \phi/2$]Sin[$\theta/2$],

Sin[$\xi - \phi/2$]Sin[$\theta/2$]]/.subs2$\}, \{\xi, 0, 2\pi\}$, PlotStyle $\to \{$Red, Blue$\}$,

PlotRange $\to$ All, Axes $\to$ False, Boxed $\to$ False];

$\{$points, circles$\}$

(*LatitudeofS^2generates$a$torusinR^3*)

sub = $\{\theta \to \pi/3\}$;

latitude = ParametricPlot3D[$\{$Sin[θ]Cos[ϕ], Sin[θ]Sin[ϕ], Cos[θ]$\}$/.sub,

$\{\phi, 0, 2\pi\}$, PlotStyle $\to \{$Thick, Blue$\}$];

torus =

ParametricPlot3D[

$s[\text{Cos}[\phi/2 + \xi]\text{Cos}[\theta/2], \text{Sin}[\phi/2 + \xi]\text{Cos}[\theta/2], \text{Cos}[\xi - \phi/2]\text{Sin}[\theta/2],$

$\text{Sin}[\xi - \phi/2]\text{Sin}[\theta/2]]/.\text{sub}, \{\phi, 0, 2\pi\}, \{\xi, 0, 2\pi\}, \text{PlotStyle} \to \{\text{Opacity}[.5], \text{Blue}\},$

$\text{Mesh} \to \text{None}];$

$\text{circle} = \text{Graphics3D}[\{\text{Yellow}, \text{Opacity}[.5], \text{Sphere}[\{0, 0, 0\}]\}];$

$\{\text{Show}[\{\text{circle}, \text{latitude}\}, \text{PlotRange} \to \text{All}, \text{Boxed} \to \text{False}, \text{Axes} \to \text{False}],$

$\text{Show}[\text{torus}, \text{PlotRange} \to \text{All}, \text{Boxed} \to \text{False}, \text{Axes} \to \text{False}]\}$

(*The Hopf Fibration*)

$\text{number} = 20;$

$\text{subs} = \{\eta 1 \to \pi/4, \eta 2 \to \pi/2, \eta 3 \to 3\pi/4\};$

$\text{points} = \text{Graphics3D}[\{\text{Opacity}[.2], \text{Sphere}[\{0, 0, 0\}], \text{PointSize}[\text{Medium}],$

$\text{Opacity}[1], \text{Red},$

$\text{Point}[\text{Table}[\{\text{Sin}[\eta 1]\text{Cos}[\xi 1], \text{Sin}[\eta 1]\text{Sin}[\xi 1], \text{Cos}[\eta 1]\}/.\text{subs},$

$\{\xi 1, 0, 3\pi/2, \pi/(\text{number})\}]], \text{Green},$

$\text{Point}[\text{Table}[\{\text{Sin}[\eta 2]\text{Cos}[\xi 1], \text{Sin}[\eta 2]\text{Sin}[\xi 1], \text{Cos}[\eta 2]\}/.\text{subs},$

$\{\xi 1, 0, 3\pi/2, \pi/(\text{number})\}]], \text{Blue},$

$\text{Point}[\text{Table}[\{\text{Sin}[\eta 3]\text{Cos}[\xi 1], \text{Sin}[\eta 3]\text{Sin}[\xi 1], \text{Cos}[\eta 3]\}/.\text{subs},$

$\{\xi 1, 0, 3\pi/2, \pi/\text{number}\}]]\}];$

$\text{red} = \text{ParametricPlot3D}[$

$\text{Table}[s[\text{Cos}[\xi 1/2 + \xi 2]\text{Cos}[\eta 1/2], \text{Sin}[\xi 1/2 + \xi 2]\text{Cos}[\eta 1/2], \text{Cos}[\xi 2 - \xi 1/2]\text{Sin}[\eta 1/2],$

$\text{Sin}[\xi 2 - \xi 1/2]\text{Sin}[\eta 1/2]]/.\text{subs}, \{\xi 1, 0, 3\pi/2, \pi/(\text{number})\}], \{\xi 2, 0, 2\pi\},$

$\text{PlotRange} \to \text{All}, \text{PlotStyle} \to \text{Red}];$

$\text{green} =$

ParametricPlot3D[

$\text{Table}[s[\text{Cos}[\xi 1/2 + \xi 2]\text{Cos}[\eta 2/2], \text{Sin}[\xi 1/2 + \xi 2]\text{Cos}[\eta 2/2], \text{Cos}[\xi 2 - \xi 1/2]\text{Sin}[\eta 2/2],$

$\text{Sin}[\xi 2 - \xi 1/2]\text{Sin}[\eta 2/2]]/.\text{subs}, \{\xi 1, 0, 3\pi/2, \pi/(\text{number})\}], \{\xi 2, 0, 2\pi\},$

PlotRange $\to$ All, PlotStyle $\to$ Green];

blue =

ParametricPlot3D[

Table[s[Cos[ξ1/2 + ξ2]Cos[η3/2], Sin[ξ1/2 + ξ2]Cos[η3/2], Cos[ξ2 − ξ1/2]Sin[η3/2],

Sin[ξ2 − ξ1/2]Sin[η3/2]]/.subs, {ξ1, 0, 3π/2, π/number}], {ξ2, 0, 2π},

PlotRange $\to$ All, PlotStyle $\to$ Blue];

{Show[points, PlotRange $\to$ All, Boxed $\to$ False, Axes $\to$ False],

Show[{red, green, blue}, PlotRange $\to$ All, Axes $\to$ False, Boxed $\to$ False]}

References

[1] C. C. Adams. *The Knot Book.* American Mathematical Society, 2004.

[2] H. Bateman. *The Mathematical Analysis of Electrical and Optical Wave-Motion.* Cambridge: University Press, 1915.

[3] I. Bialynicki-Birula. Electromagnetic vortex lines riding atop null solutions of the maxwell equations. *Journal of Optics A: Pure and Applied Optics*, 6, 2004.

[4] S. Das Sarma, M. Freedman, and C. Nayak. Topological quantum computation. *Physics Today*, 59(7), 2006.

[5] H. Hopf. Über die abbildungen der dreidimensionalen sphäre auf die kugelfläche. *Mathematische Annalen*, 104, 1931.

[6] W. T. M. Irvine. Linked and knotted beams of light, conservation of helicity and the flow of null electromagnetic fields. *Journal of Physics A: Mathematical and Theoretical*, 43, 2010.

[7] W. T. M. Irvine and D. Bouwmeester. Linked and knotted beams of light. *Nature Physics*.

[8] H. Kedia, I. Bialynicki-Birula, D. Peralta-Salas, and W. T. M. Irvine. Tying knots in light fields. *Physical Review Letters*, 111, 2013.

[9] L. C. Kinsey. *Topology of Surfaces.* Springer, 1993.

[10] A. Kitaev. Fault-tolerant quantum computation by anyons. *Annals of Physics*, 303(1), 2003.

[11] L. Landau and E. Lifshitz. *Course of Theoretical Physics: Volume 2: The Classical Theory of Fields, 4th Edition.* Butterworth-Heinemann, 1975.

[12] D. W. Lyons. An elementary introduction to the hopf fibration. *Mathematical Magazine*, 76(2), 2003.

[13] J. Milnor. *Singular Points of Complex Hypersurfaces.* Princeton University Press, 1969.

[14] A. F. Rañada. A topological theory of the electromagnetic field. *Letters in Mathematical Physics*, 18, 1989.

[15] A. F. Rañada. Knotted solutions of the maxwell equations in vacuum. *Journal of Physics A: Mathematical and General*, 23(16), 1990.

[16] I. Robinson. Null electromagnetic fields. *Journal of Mathematical Physics*, 2(3), 1961.

[17] H. Seifert. Über das geschlecht von knoten. *Mathematische Annalen*, 110, 1935.

[18] W. Thomson. On vortex atoms. *Philosophical Magazine*, XXXIV, 1867.

[19] E. Witten. Quantum field theory and the jones polynomial. *Communications in Mathematical Physics*, 121(3), 1989.

Curriculum Vitae

Personal Information

Name: John Waite

Email: jvw831@gmail.com

Phone: (702) 708-0444

Education

Graduation Date	Degreee Awarded	Institution
May 2016	MS - Physics	University of Nevada, Las Vegas
August 2010	BS - Mathematics	University of Maryland, College Park